An Image Sharpening Operator Combined with Framelet for Image Deblurring

Jingjing Liu[1], **Yifei Lou**[2], **Guoxi Ni**[3], **Tieyong Zeng**[4]

[1] *School of Mathematical Sciences, Peking University, Beijing, 100871, China*
[2] *Department of Mathematical Sciences, University of Texas at Dallas, Dallas, TX 75080*
[3] *LCP, Institute of Applied Physics and Computational Mathematics, Beijing, 100088, China*
[4] *Department of Mathematics, The Chinese University of Hong Kong, Shatin, N.T., Hong Kong*

E-mail: Yifei.Lou@utdallas.edu, zeng@math.cuhk.edu.hk

June 2019

Abstract. Image sharpening can highlight fine details in images but with a tendency of amplifying noise. This paper proposes a novel idea of incorporating an image sharpening operator into a framelet-based model for image deblurring. The proposed model is convex and hence it can be solved efficiently by the semi-proximal alternating direction method of multipliers (sPADMM) with guaranteed linear rate convergence, which covers the classical ADMM. The experimental results on different blurring kernels and Gaussian noise levels show that the proposed approach outperforms the state-of-the-art methods in terms of PSNR, SSIM, relative error, and visual quality.

Keywords: image sharpening, wavelet frame, image restoration, semi-proximal alternating direction method of multipliers

1. Introduction

In the process of image acquisition and transmission, blurring is inevitable due to optical degradation, object motion, and air turbulence [1–4]. The blurring process can be regarded as diffusion that smears out original (sharp) images. For example, a forward heat equation is a typical diffusion process [5]. As the backward heat equation is known to be notoriously unable, the deblurring problem (to undo the blur) is highly ill-posed.

One of popular methods in image deblurring involves a regularization term that regularizes the solution and refines the feasible set. Among various regularization models, *e.g.*, [6–14], the Rudin-Osher-Fatemi (ROF) model [15] that minimizes the total variation (TV) is widely used. It is true that the ROF model can preserve edges, but it is unable to distinguish a jump (a sharp image) from a smooth transition (a

blurred version), as both have the same value of total variation. Therefore, the TV regularization results in a suboptimal effect on image deblurring.

On the other hand, a direct approach for image deblurring focuses on the backward diffusion. For example, Osher and Rudin [16] proposed a shock filter that creates a shock during diffusion for the purpose of image sharpening. Although this approach sounds severely unstable, Rudin and Osher provided a sophisticated numerical scheme that yields reasonable results. Alvarez and Mazorra [17] later combined the shock filter with an anisotropic diffusion to stabilize the solution. Alternatively, Gilboa *et al.* [18] proposed a forward and backward diffusion model for image sharpening and denoising. Recently, Calder *et al.* [19] considered a Sobolev gradient flow for image sharpening, which will be elaborated later due to its relevance of the proposed approach. Generally speaking, one major drawback for image sharpening methods is the tendency of amplifying the noise due to the inherent instability.

In this paper, we innovatively propose to combine image sharpening with a regularization approach. In particular, we rely on an image sharpening operator to enhance and reveal important features in an image. We then formulate a framelet-based model to stabilize the image deblurring process, thus leading to a sharp and satisfactory recovery. The two-step approach results in a convex minimization problem, which can be solved efficiently by the semi-proximal alternating direction method of multipliers (sPADMM) [20–22] with a linear-rate convergence. One important advantage of the sPADMM algorithm is its potential to deal with any subproblems that do not have closed-form solutions. The main contributions of this work are three-fold,

(1) We combine image sharpening with a regularization-based method for image deblurring, which is better than applying either one alone.
(2) We propose a convex optimization model that enables an efficient numerical algorithm of sPADMM with guaranteed convergence.
(3) We conduct extensive experiments to demonstrate that the proposed method outperforms the state-of-the-art methods in image deblurring.

The rest of the paper is organized in the following way. Section 2 devotes to the literature review of regularization methods and an image sharpening operator. In Section 3, we propose our model by combining the image sharpening operator with a regularization method. We also establish the existence and uniqueness of the model solution and describe an efficient sPADMM algorithm to find the solution with convergence analysis. Experimental results are exhibited in Section 4, followed by conclusions and future works in Section 5.

2. Literature review

We describe an image degradation [23–26] as follows,

$$f = Au + \varepsilon, \tag{2.1}$$

where A represents a (linear) blurring operator, u is an (unknown) original image, f is an observed image, and ε is often assumed to be Gaussian noise with zero mean and standard deviation σ. Image deblurring aims to recover a sharp image u given the blurring operator A and the blurry and noisy input f. We will review some regularization methods in the literature of image deblurring, followed by the Sobolev gradient flow [19] for image sharpening.

2.1. Regularization methods

The ROF model can be expressed

$$\min_u \frac{\lambda}{2}\|Au - f\|_2^2 + \|Du\|_1, \tag{2.2}$$

where D denotes a derivative operator, $\|Du\|_1$ is the total variation of the image u, and λ is a positive parameter to balance between a good fit and a regularized solution. Note that there are isotropic TV and anisotropic TV formulations depending on how the l_1-norm is defined.

There are numerous efficient algorithms for solving the TV-regularized deblurring model such as [27–30]. Specifically in [30], Wang *et al.* considered an approximated model of (2.2) by introducing an auxiliary variable at each pixel $\mathbf{w} \in \mathbb{R}^2$ to represent Du,

$$\min_{\mathbf{w},u} \frac{\lambda}{2}\|Au - f\|_2^2 + \frac{\beta}{2}\|\mathbf{w} - Du\|_2^2 + \|\mathbf{w}\|_2, \tag{2.3}$$

where β is a sufficiently large penalty parameter. Since this formulation enables the closed-form solution of each sub-problem, it has advantages of low computational complexity and high numerical stability, thus referred to as *fast total variation deconvolution* (FTVd). This algorithm was later explored in other imaging applications [31–33].

Lou *et al.* [34] proposed a weighted difference of anisotropic and isotropic total variation, denoted by *ani-iso TV*, as a regularization term for image processing,

$$\min_u \frac{\lambda}{2}\|Au - f\|_2^2 + \|D_x u\|_1 + \|D_y u\|_1 - \alpha\|\sqrt{|D_x u|^2 + |D_y u|^2}\|_1, \tag{2.4}$$

with a parameter $\alpha \in [0, 1]$. The idea is stemmed from an $l_1 - \alpha l_2$ penalty [35–38] that works particularly well for recovering sparse vectors. Similar idea is considered in [39] that borrows minimax concave penalty (MCP) [40] from compressed sensing to image processing.

Other than gradient-based regularizations, wavelet frame based approaches are also widely used due to its multiresolution structure, sparse representations, and high redundancy [41–47]. Note that there are several different types of wavelet models, including synthesis based approaches [48, 49], analysis based approaches [50, 51], and balanced approaches [52, 53]. Specifically in [43], Cai *et al.* considered the l_1-norm in the wavelet tight frame transform domain, i.e.,

$$\min_u \frac{\lambda}{2}\|Au - f\|_2^2 + \|Wu\|_1, \tag{2.5}$$

where W is the framelet transform satisfying $W^TW = I$ with the identity matrix I. This approach is referred to as the *framelet* method.

2.2. Sharpening operator

We provide a brief review on the Sobolev gradient flow [19] that can be used for image sharpening. It is well-know that the heat equation of $u_t = \Delta u$ is the gradient descent flow for minimizing the functional $E(u) = \frac{1}{2}\int_\Omega \|\nabla u\|^2 = \frac{1}{2}\|\nabla u\|_2^2$ with respect to the standard Euclidean metric, where Ω is an open subset of $\mathbb{R}^2$ with smooth boundary $\partial\Omega$. Sundaramoorthi *et al.* [54] considered an inner product on the Sobolev space $H^1(\Omega)$ [55], defined as $\langle v, w\rangle \longrightarrow g_\tau(v, w) = (1-\tau)\langle v, w\rangle_{L^2} + \tau\langle v, w\rangle_{H^1}$ for any $\tau > 0$. As a result, the gradient of $E(u)$ with respect to the Sobolev metric g_τ is given by

$$\nabla_{g_\tau} E|_u = -\Delta(I - \tau\Delta)^{-1}u,$$

where I denotes the identity operator with an abuse notation of the identity matrix. Unlike the backward heat equation that is extremely unstable, the backward Sobolev gradient flow defined by

$$u_t = \Delta(I - \tau\Delta)^{-1}u, \tag{2.6}$$

is well-posed [56]. As the backward direction can be used for image sharpening, Calder *et. al.* [19] proposed to minimize the following functional,

$$F(u) = \frac{1}{4}\|\nabla u_0\|_2^2\left(\frac{\|\nabla u\|_2^2}{\|\nabla u_0\|_2^2} - \gamma\right)^2, \tag{2.7}$$

where u_0 is the initial condition and γ is the sharpness factor in the sense that the recoverred image looks blurring for $\gamma < 1$ and gets sharpened for $\gamma > 1$. Note that a larger γ value corresponds to a sharper reconstruction.

It is straightforward to derive a gradient descent flow for minimizing (2.7) with respect to the Sobolev metric g_τ, i.e.,

$$u_t = \left(\frac{\|\nabla u\|_2^2}{\|\nabla u_0\|_2^2} - \gamma\right)\Delta(I - \tau\Delta)^{-1}u. \tag{2.8}$$

This is a nonlinear PDE with a natural stopping time when the ratio of $\|\nabla u\|_2^2$ and $\|\nabla u^0\|_2^2$ reaches to γ.

3. Our Approach

We propose to use the image sharpening operator to recover finer structures from a blurred input, which can be regarded as a preprocessing step. As the solution of (2.8) is unique [56], we denote $B(\cdot)$ as an operator that takes an initial condition u_0 and outputs the steady-state solution $B(u_0)$ corresponding to the PDE (2.8). Then, we utilize the wavelet frame approach to further improve upon the image restoration result. As such, we propose the following model

$$\min_u \frac{\lambda}{2}\|Au - f\|_2^2 + \|Wu\|_1 + \mu\|u - B(f)\|_1, \tag{3.1}$$

where W is the framelet transform, $B(f)$ is a sharpened image, and λ, μ are two positive parameters. We use the l_2 norm for the data fitting term by the assumption that the noise term η in (2.1) follows the Gaussian distribution. The second term in the proposed model (3.1) is measured by the l_1 norm in order to suppress the erroneous artifacts [57] caused by the sharpening operator (the l_2 norm may smear out the result). Denoting $g = B(f)$, we rewrite the proposed model (3.1) as follows:

$$\min_u \mathcal{J}(u) \equiv \frac{\lambda}{2}\|Au - f\|_2^2 + \|Wu\|_1 + \mu\|u - g\|_1. \tag{3.2}$$

We establish the existence of the problem (3.2) in Theorem 3.1. If null space of A only contains zero, then the problem (3.2) has a unique minimizer. Recall the definition of *coerciveness* [60] as follows:

Definition 3.1 *A functional $\mathcal{J} : X \to \mathbb{R}$ on a Banach space X is called coercive if $\|u^k\| \to +\infty$ implies $\mathcal{J}(u^k) \to +\infty$ for every sequence $\{u^k\}_{k\in N} \subset X$.*

The existence of a solution to the model (3.2) is based on a theorem in [60], stating that any continuous, convex, and coercive functional on a Banach space has a global minimizer.

Theorem 3.1 *There exists a global minimizer of the objective functional in (3.2).*

Proof It is obvious that both l_2 and l_1 norms are continuous and convex on the Banach Space L^2, so is $\mathcal{J}(u)$. Additionally for any sequence $\|u^k\|_2 \to +\infty$, we have $\|Wu^k\|_1, \|u^k - g\|_1$, and $\|Au^k - f\|_2^2$ go to infinity, so $\mathcal{J}(u)$ is coercive and hence $\mathcal{J}(u)$ has a global minimizer. □

In what follows, we describe the semi-proximal alternating direction method of multipliers (sPADMM), which has the potential to deal with any subproblems that do not have closed-form solutions. In order to apply sPADMM, we express the minimization problem (3.2) as an equivalent form,

$$\min_{u,d,z} \frac{\lambda}{2}\|Au - f\|_2^2 + \|d\|_1 + \mu\|z\|_1 \;\; s.t.\; Wu - d = 0,\; u - g - z = 0. \tag{3.3}$$

The augmented Lagrangian function of problem (3.3) is formulated by

$$\begin{aligned}\mathcal{S}(u, d, z; b, c) = &\frac{\lambda}{2}\|Au - f\|_2^2 + \|d\|_1 + \mu\|z\|_1 \\ &+ \frac{\mu_1}{2}\|Wu - d\|_2^2 + \langle Wu - d, b\rangle \\ &+ \frac{\mu_2}{2}\|u - g - z\|_2^2 + \langle u - g - z, c\rangle,\end{aligned} \tag{3.4}$$

where $\mu_1, \mu_2 > 0$ are two penalty parameters and b, c are the Lagrange multipliers. The sPADMM iteration for solving (3.4) goes as follows,

$$\begin{cases} u^{k+1} \in \arg\min_u \mathcal{S}(u, d^k, z^k; b^k, c^k) + \frac{1}{2}\|u - u^k\|_{S_1}^2 \\ d^{k+1} \in \arg\min_d \mathcal{S}(u^{k+1}, d, z^k; b^k, c^k) + \frac{1}{2}\|d - d^k\|_{S_2}^2 \\ z^{k+1} \in \arg\min_z \mathcal{S}(u^{k+1}, d^{k+1}, z; b^k, c^k) + \frac{1}{2}\|z - z^k\|_{S_3}^2 \\ b^{k+1} = b^k + \eta\mu_1(Wu^{k+1} - d^{k+1}) \\ c^{k+1} = c^k + \eta\mu_2(u^{k+1} - g - z^{k+1}). \end{cases} \tag{3.5}$$

Here the matrix norm is defined as $\|x\|_M = \sqrt{\langle x, Mx\rangle}$ for any $x \in \mathcal{X}$ and self-adjoint positive semidefinite linear operator $M : \mathcal{X} \to \mathcal{X}$. As a result, the alternating direction method of multipliers (ADMM) [61–64] is a special case of sPADMM by setting $S_1 = 0, S_2 = 0$, and $S_3 = 0$. If one chooses strictly positive definite matrices S_1, S_2, S_3, then it is more efficient to solve the subproblems with a guaranteed linear rate convergence for $\eta \in (0, (1+\sqrt{5})/2)$ under mild conditions.

Next, we elaborate how to solve these subproblems respectively. The u-subproblem is written as

$$\begin{aligned} u^{k+1} = \arg\min_u \frac{\lambda}{2}\|Au - f\|_2^2 + \langle b^k, Wu - d^k\rangle + \frac{\mu_1}{2}\|Wu - d^k\|_2^2 \\ + \langle c^k, u - g - z^k\rangle + \frac{\mu_2}{2}\|u - g - z^k\|_2^2 + \frac{1}{2}\|u - u^k\|_{S_1}^2. \end{aligned} \tag{3.6}$$

The optimality condition of (3.6) is given by

$$\begin{aligned} 0 = \lambda A^T(Au - f) + \mu_1 W^T(Wu - d^k + \frac{b^k}{\mu_1}) \\ + \mu_2(u - g - z^k + \frac{c^k}{\mu_2}) + S_1(u - u^k). \end{aligned} \tag{3.7}$$

Since $W^TW = I$, we obtain the following linear system,

$$\begin{aligned} \Big(\lambda A^TA + (\mu_1 + \mu_2)I + S_1\Big)u = \lambda A^Tf + \mu_1 W^T(d^k - b^k) \\ + \mu_2(g + z^k - c^k) + S_1(u^k). \end{aligned} \tag{3.8}$$

Under the periodic boundary condition (BC) for u, we know that A^TA, and A^Tf are block circulant, the Hessian matrix on the left-hand of (3.8) can be diagonalized by two-dimensional discrete Fourier transform $\mathcal{F}$. Using the convolution theorem of Fourier transforms, the solution of (3.8) can be written as

$$\begin{aligned} u^{k+1} = \mathcal{F}^{-1} \\ \left(\frac{\lambda\mathcal{F}(A)^* \circ \mathcal{F}(f) + \mu_1\mathcal{F}(W)^* \circ \mathcal{F}(d^k - b^k) + \mu_2\mathcal{F}(g + z^k - c^k) + \mathcal{F}(S_1) \circ \mathcal{F}(u^k)}{\lambda\mathcal{F}(A)^* \circ \mathcal{F}(A) + \mu_1 + \mu_2 + \mathcal{F}(S_1)}\right), \end{aligned} \tag{3.9}$$

where $*$ denotes complex conjugation, $\circ$ means component-wise multiplication, and the division is component-wise as well. There are analogous fast transforms for other boundary conditions [65]. For example, the blurring operator corresponding to reflective BC can be diagonalized by the fast cosine transform and the one for anti-reflective BC can be diagonalized by the fast sine transform.

The d-subproblem is equivalent to

$$d^{k+1} = \arg\min_d \|d\|_1 - \langle b^k, d - Wu^{k+1}\rangle + \frac{\mu_1}{2}\|d - Wu^{k+1}\|_2^2 + \frac{1}{2}\|d - d^k\|_{S_2}^2. \tag{3.10}$$

The solution of d can be obtained by

$$d^{k+1} = \mathcal{T}_{1/(\mu_1 + \lambda_{max}(S_2))}\Big(\frac{\mu_1 Wu^{k+1} + b^k + S_2d^k}{\mu_1 + \lambda_{max}(S_2)}\Big), \tag{3.11}$$

where $\lambda_{max}(S_2)$ denotes the largest eigenvalue of the matrix S_2 and the operator $\mathcal{T}_\theta$ is a *soft shrinkage* operator defined component-wisely as

$$(\mathcal{T}_\theta(x))_i = \mathrm{sgn}(x_i) * \max(|x_i| - \theta, 0).$$

Algorithm 1 sPADMM for minimizing the proposed model (3.2).

Step 1: Given a blurring operator A and a blurred noisy input f.
Step 2: Set parameters $\gamma, \tau, \lambda, \mu, \mu_1, \mu_2, \eta$ and stopping parameters *tol* and kMax.
Step 3: Run (2.8) until the steady state to obtain g.
Step 4: Initialize $u^0 = f$ and $d^0 = b^0 = z^0 = c^0 = 0$.
For $k = 0, 1, 2, \cdots$,kMax, iterate

$$\begin{cases} u^{k+1} = \mathcal{F}^{-1}\left(\frac{\lambda\mathcal{F}(A)^*\circ\mathcal{F}(f)+\mu_1\mathcal{F}(W)^*\circ\mathcal{F}(d^k-b^k)+\mu_2\mathcal{F}(g+z^k-c^k)+\mathcal{F}(S_1)\circ\mathcal{F}(u^k)}{\lambda\mathcal{F}(A)^*\circ\mathcal{F}(A)+\mu_1+\mu_2+\mathcal{F}(S_1)}\right), \\ d^{k+1} = \mathcal{T}_{1/(\mu_1+\lambda_{max}(S_2))}\left(\frac{\mu_1 W u^{k+1}+b^k+S_2 d^k}{\mu_1+\lambda_{max}(S_2)}\right), \\ z^{k+1} = \mathcal{T}_{\mu/(\mu_2+\lambda_{max}(S_3))}\left(\frac{(\mu_2(u^{k+1}-g)+c^k+S_3 z^k)}{\mu_2+\lambda_{max}(S_3)}\right), \\ b^{k+1} = b^k + \eta\mu_1(Wu^{k+1} - d^{k+1}), \\ c^{k+1} = c^k + \eta\mu_2(u^{k+1} - g - z^{k+1}). \end{cases}$$

Step 5: If $\|u^{(k+1)} - u^{(k)}\|/\|u^{(k+1)}\| \le tol$, stop.
Step 6: Output $u^{(k+1)}$.

For the z-subproblem, we have

$$\begin{aligned} z^{k+1} = \arg\min_z \mu\|z\|_1 - \langle c^k, z - (u^{k+1} - g)\rangle \\ + \frac{\mu_2}{2}\|z - (u^{k+1} - g)\|_2^2 + \frac{1}{2}\|z - z^k\|_{S_3}^2, \end{aligned} \tag{3.12}$$

which can be solved by the soft shrinkage as well, i.e.,

$$z^{k+1} = \mathcal{T}_{\mu/(\mu_2+\lambda_{max}(S_3))}\Big(\frac{(\mu_2(u^{k+1} - g) + c^k + S_3 z^k)}{\mu_2 + \lambda_{max}(S_3)}\Big). \tag{3.13}$$

The overall algorithm is summarized in Algorithm 1. The linear-rate convergence of the proposed algorithm is characterized in Theorem 3.2. Please refer to Appendix for the proof.

Theorem 3.2 *Let $\{(u^k, d^k, z^k, b^k, c^k)\}$ are generated from the sPADMM. If $\eta \in (0, (1+\sqrt{5})/2)$, then the whole sequence $\{(u^k, d^k, z^k, b^k, c^k)\}$ converges to the KKT point.*

4. Experimental results

In this section, we present various deblurring results using six testing images, labelled by Boat (256×256), Cameraman (256×256), Goldhill (256×256), House (256×256), Man (512×512), and Plate (200×380), as showed in Figure 1.

We consider three types of blurring functions with Matlab commands:

- average blur (AB): `fspecial('average',hsize)`;
- Gaussian blur (GB): `fspecial ('gaussian',hsize,sigma)`;
- motion blur (MB): `fspecial('motion',len,theta)`.

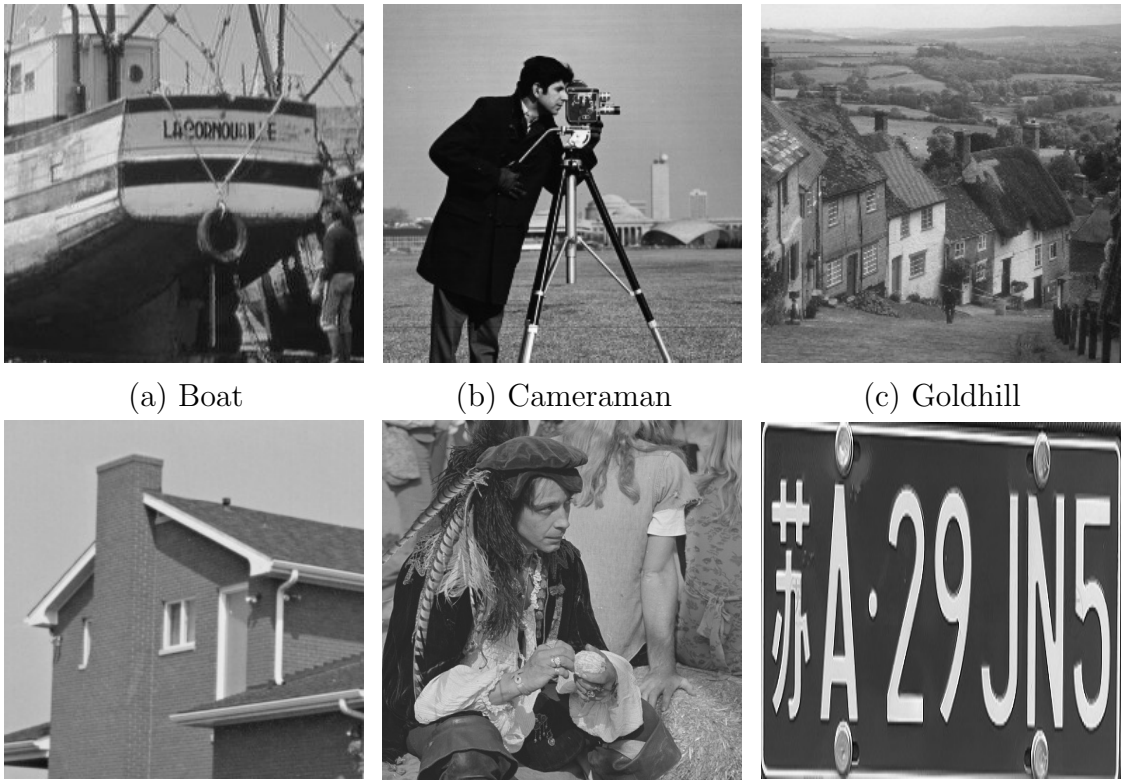

(a) Boat (b) Cameraman (c) Goldhill

(d) House (e) Man (f) Plate

Figure 1: Testing images.

For AB and GB, the blurring kernels to be tested are of size 5×5, 7×7, and 9×9. The standard deviations in GB are `sigma`=2, 3, and 4. As for MB, we use `len`=9, 15, and 20 with an angle `theta`=30, 45, 60, 120. Furthermore, Gaussian noise is added to blurred images with a standard deviation of 1, 3, 5, or 10. We use the notation of AB(5,5)/$\sigma = 1$ to denote the case of average blur of size 5×5 and Gaussian noise of the standard deviation $\sigma = 1$. Similarly, we use GB(9,4)/$\sigma = 5$ for Gaussian kernel of size 9×9 and standard deviation of 4 with additive Gaussian noise of standard deviation of $\sigma = 5$. The motion blur of size 20×20 with additive Gaussian noise of standard deviation of $\sigma = 10$ is denoted as MB(20,120)/$\sigma = 10$.

To illustrate the effectiveness of the proposed approach, we compare with the following image deblurring algorithms,

- **TV** [30] used alternating direction method (ADM) to solve the ROF model (2.2);
- **Framelet** [43] is based on the wavelet frame and solved by the split Bregman(SB) algorithm;
- **ani-iso TV** [34] is a weighted difference of anisotropic and isotropic TV as the regularization and solved via a difference of convex algorithm (DCA);
- **BM3D** deblurring [68] is a two-stage non-iterative algorithm that is built on the famous BM3D denoising filter [69] with a regularized Wiener inversion to get the

final deblurred image.

Quantitatively, we evaluate the quality of image restoration by peak signal-to-noise ratio (PSNR), relative error (ReErr), and structural similarity (SSIM) [70]. PSNR and ReErr are defined as,

$$\text{PSNR} = 10\log_{10}\frac{255^2 p}{\|\tilde{u}-u\|_2^2}, \quad \text{ReErr} = \frac{\|\tilde{u}-u\|_2^2}{\|u\|_2^2},$$

where $u,\ \tilde{u},\ p$ denote the original image, the restored image, and the number of pixels in the image, respectively. As for SSIM, we define local similarity index computed on windows x and y,

$$ssim(x,y) = \frac{(2\mu_x\mu_y + c_1)(2\sigma_{xy} + c_2)}{(\mu_x^2 + \mu_y^2 + c_1)(\sigma_x^2 + \sigma_y^2 + c_2)},$$

where μ_x, μ_y are the average of x, y, σ_x^2, σ_y^2 are the variance, $\sigma_{x,y}$ is the covariance of x, y, and c_1, c_2 are two variables to stabilize the division with weak denominator. The overall SSIM is the mean of local similarity indexes,

$$\text{SSIM} = \frac{1}{N}\sum_{i=1}^{N} ssim((x_i, y_i)),$$

where x_i, y_i are corresponding windows of original/restored image indexed by i and N is the number of windows. Here, we consider the windows of size 8×8. Note that larger PSNR, larger SSIM, and smaller ReErr values mean better restored results. All the experiments are performed under Windows 7 and MATLAB R2014a running on a desktop (Intel(R) Core(TM) i7-4790 CPU @ 3.60GHz).

4.1. Parameter settings

We summarize the role of each parameter in our algorithm. In the pre-computing step (i.e., image sharpening), there are two parameters τ and γ that control the sharpening effect. Though they should be adjusted for different blurring kernels, we observe that $\tau = 5$, $\gamma = 5$ usually give reasonable results and hence we fix these values in all experiments. In addition, there are parameters $(\lambda, \mu, \mu_1, \mu_2, \eta)$ in our algorithm (3.4). The parameter λ balances the data-fitting term and the regularization term. A larger value of λ yields unsatisfactory denoising results. If λ is too small, the recovered image suffers from over-smoothing. A rule of thumb is that a smaller λ value is used for a noisier input. We choose the best λ from the set of $\{2, 3, 4, 5, 6, 7, 8, 9, 10, 11, 12, 13, 14, 35, 36, 37, 38, 40, 45\}$. The parameter μ reflects how much we trust the sharpened image. We choose the best value of μ among the set of $\{1e-4, 1e-3, 1e-2\}$. As for algorithmic parameters μ_1 and μ_2 that only affect the convergence speed, we fix the values as $\mu_1 = 0.2$, and $\mu_2 = 1e-1$. We choose the self-adjoint positive semidefinite linear operators $S_1 = S_2 = S_3 = \rho I$ and $\rho \in \{0.1, 0.2, 0.3\}$. The step-length η is set to be $1.6 \in (0, (1+\sqrt{5})/2)$ for guaranteed convergence. In all the experiments, the stop criterion is either $\frac{\|u^{k+1}-u^k\|_2}{\|u^k\|_2} < 1e^{-4}$ or the maximum iterative number exceeds 1000. According to the above setting of parameters, we plot the PSNR

values and the objective function values $\mathcal{J}(u)$ versus the iteration numbers in Figure 2, which empirically shows the convergence of the sPADMM algorithm and our stopping criteria are reasonable.

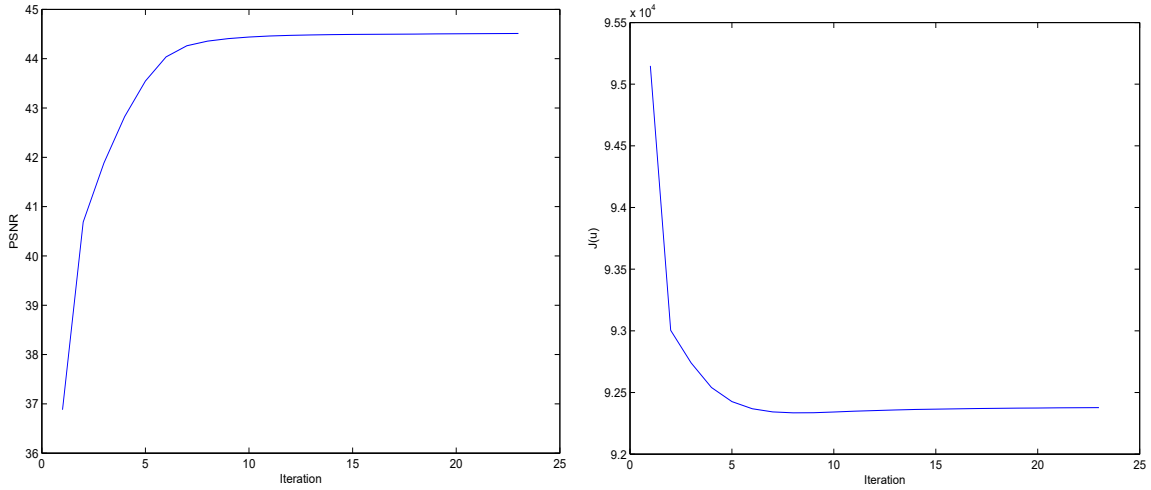

(a) PSNR value versus iteration number (b) J(u) value versus iteration number

Figure 2: The PSNR and $\mathcal{J}(u)$ versus the iteration number for House image corrupted by GB(7,3)/$\sigma = 3$.

We describe the parameter settings for these competing methods. Specifically for the TV method, its model (2.3) involves two parameters (λ, β). The parameter λ is the trade-off between data fitting and regularization terms, while β affects the convergence of the algorithm. We choose the best combination of $\lambda \in \{0.5, 1, 2, 3, 5, 20, 25\}$ and $\beta \in \{0.4, 0.5, 0.8, 1, 8, 16\}$. The parameters used in framelet method (2.5) are set as $\lambda \in \{2, 4, 6, 7, 10, 30\}$ and $\mu \in \{0.005, 0.01, 0.003, 0.005\}$. As for ani-iso TV, we fix $\alpha = 0.5$ and set other parameters as $\mu \in \{0.5, 1.5, 3, 15\}$ and $\lambda \in \{0.1, 0.5\}$. The BM3D method requires two parameters, referred to as regularized inversion (RI) with collaborative hard-thresholding and regularized Wiener inversion (RWI) with collaborative Wiener filtering. We choose two parameters as RI $\in \{1e-4, 5e-4, 5e-3, 1e-3, 1e-2\}$ and RWI $\in \{5e-3, 3e-3, 2e-3\}$.

4.2. Simplified models

Before presenting the deblurring results of the proposed model, we want to highlight each term in the proposed model (3.2) is influential. For this purpose, we present the comparison results of the standard wavelet method (2.5), without tightframe, and without the data fitting term.

The standard wavelet method based on the sharpened image is formulated as follows,

$$\min_u \frac{\lambda}{2}\|Au - f\|_2^2 + \|Wu\|_1. \tag{4.1}$$

To apply the ADMM approach, we introduce an auxiliary variable $d = Wu$ and formulate the augmented Lagrangian,

$$\min_{u,d} \frac{\lambda}{2}\|Au - f\|_2^2 + \|d\|_1 + \mu_1\langle Wu - d, b\rangle + \frac{\mu_1}{2}\|Wu - d\|_2^2. \tag{4.2}$$

The ADMM iteration is expressed as

$$\begin{cases} u^{k+1} = (\lambda A^T A + \mu_1)^{-1}(\lambda A^T f + \mu_1 W^T(d^k - b^k)) \\ d^{k+1} = \mathcal{T}_{\frac{1}{\mu_1}}(Wu^{k+1} + b^k) \\ b^{k+1} = b^k + Wu^{k+1} - d^{k+1}. \end{cases} \tag{4.3}$$

To make a fair comparison to the proposed approach, we consider the use of the sharpened image g as an initial condition for (4.3).

The model without tight frame is reduced to

$$\min_u \frac{\lambda}{2}\|Au - f\|_2^2 + \mu\|u - g\|_1, \tag{4.4}$$

and the ADMM algorithm iterates as follows,

$$\begin{cases} u^{k+1} = (\lambda A^T A + \mu_2)^{-1}(\lambda A^T f + \mu_2(g + z^k - c^k)) \\ z^{k+1} = \mathcal{T}_{\frac{\mu}{\mu_2}}(u^{k+1} - g + c^k) \\ c^{k+1} = c^k + u^{k+1} - g - z^{k+1}. \end{cases} \tag{4.5}$$

Finally, we can formulate the model without data fitting term, i.e.,

$$\min_u \mu\|u - g\|_1 + \|Wu\|_1, \tag{4.6}$$

with the ADMM iterations,

$$\begin{cases} u^{k+1} = (\mu_1 + \mu_2)^{-1}(\mu_1 W^T(d^k - b^k) + \mu_2(g + z^k - c^k)) \\ d^{k+1} = \mathcal{T}_{\frac{1}{\mu_1}}(Wu^{k+1} + b^k) \\ b^{k+1} = b^k + Wu^{k+1} - d^{k+1} \\ z^{k+1} = \mathcal{T}_{\frac{\mu}{\mu_2}}(u^{k+1} - g + c^k) \\ c^{k+1} = c^k + u^{k+1} - g - z^{k+1}. \end{cases} \tag{4.7}$$

The comparison of the proposed approach with these simplified models is given in Figure 3 using Cameraman and MB(9,30)/$\sigma = 1$ as an example. We can observe that the method without data fitting term almost have no effect on deblurring. Additionally, the one without framelet has severe ringing artifacts. The standard framelet approach initialized by the sharpened image is about 0.5 dB less in PSNR compared to our approach. This example shows the importance of having each term in the proposed model.

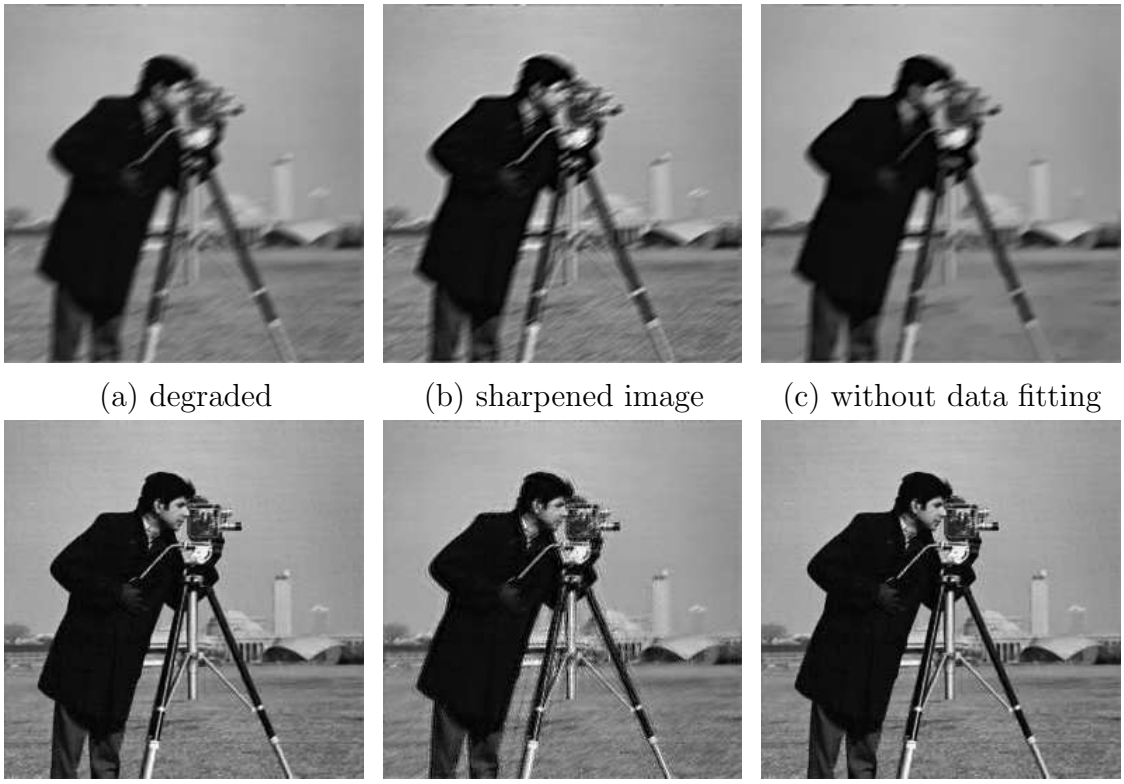

(a) degraded (b) sharpened image (c) without data fitting

(d) standard framelet (e) without framelet (f) ours

Figure 3: Comparison of simplified models for image deblurring with MB(9,30)/$\sigma = 1$. (a) Degraded image; (b) sharpened image; (c) without data-fitting: PSNR=32.16; (d) standard framelet: PSNR=44.18; (e) without framelet: PSNR=37.78; (f) Ours: PSNR=44.45.

4.3. Deblurring results

We record the values of PSNR, SSIM, ReErr of various deblurring results on average blur, Gaussian blur, and motion blur in Tables 1-3, respectively. We compare our approach with TV, Framelet, ani-iso TV, and BM3D. All the tables confirm that our proposed method achieves the best results in most of the cases. In addition, Table 4 lists the computation time, which reveals that our method is relatively slow compared to other methods. Acceleration will be left in the future work.

Table 1: PSNR (dB), SSIM, ReErr for average blur.

Image	Degraded		Input	TV	Framelet	ani-iso TV	BM3D	Ours
Boat	AB(5,5)/$\sigma = 1$	PSNR	33.62	47.06	47.21	46.86	46.53	**47.45**
		SSIM	0.759	0.924	0.930	0.919	0.929	**0.931**
		ReErr	0.0453	0.0097	0.0095	0.0099	0.0103	**0.0093**
	AB(9,9)/$\sigma = 5$	PSNR	30.12	38.13	38.69	38.35	38.84	**39.31**
		SSIM	0.503	0.742	0.769	0.749	0.765	**0.773**
		ReErr	0.0679	0.0270	0.0253	0.0263	0.0249	**0.0236**
	AB(9,9)/$\sigma = 10$	PSNR	30.05	36.71	36.95	36.88	37.45	**37.54**
		SSIM	0.369	0.688	0.700	0.697	0.717	**0.725**
		ReErr	0.0684	0.0318	0.0309	0.0311	0.0292	**0.0289**
Cameraman	AB(5,5)/$\sigma = 1$	PSNR	34.91	45.32	45.15	45.14	44.13	**45.62**
		SSIM	0.732	0.896	0.899	0.897	0.899	**0.902**
		ReErr	0.0366	0.0111	0.0113	0.0113	0.0127	**0.0109**
	AB(9,9)/$\sigma = 5$	PSNR	31.29	37.63	37.56	37.40	37.57	**38.02**
		SSIM	0.492	0.738	0.749	0.749	0.751	**0.753**
		ReErr	0.0556	0.0268	0.0270	0.0275	0.0270	**0.0256**
	AB(9,9)/$\sigma = 10$	PSNR	31.23	36.36	36.04	35.45	35.95	**36.63**
		SSIM	0.322	0.691	0.680	0.708	0.710	**0.717**
		ReErr	0.0559	0.0310	0.0322	0.0344	0.0325	**0.0301**
Goldhill	AB(5,5)/$\sigma = 1$	PSNR	33.64	46.14	45.97	46.02	46.32	**46.67**
		SSIM	0.610	0.851	0.846	0.847	0.845	**0.860**
		ReErr	0.0447	0.0106	0.0108	0.0107	0.0104	**0.0100**
	AB(9,9)/$\sigma = 5$	PSNR	30.82	38.76	38.77	38.45	39.43	**39.66**
		SSIM	0.406	0.611	0.619	0.597	0.617	**0.630**
		ReErr	0.0618	0.0248	0.0248	0.0257	0.0229	**0.0223**
	AB(9,9)/$\sigma = 10$	PSNR	30.76	36.36	36.81	36.62	36.65	**37.32**
		SSIM	0.312	0.539	0.555	0.531	0.555	**0.565**
		ReErr	0.0623	0.0326	0.0310	0.0317	0.0316	**0.0293**
House	AB(5,5)/$\sigma = 1$	PSNR	36.51	49.86	50.21	49.77	49.94	**50.42**
		SSIM	0.797	0.896	0.896	0.893	0.901	**0.902**
		ReErr	0.0269	0.0058	0.0056	0.0058	0.0057	**0.0054**
	AB(9,9)/$\sigma = 5$	PSNR	31.65	41.87	42.35	42.60	42.55	**43.14**
		SSIM	0.556	0.786	0.807	0.804	0.807	**0.816**
		ReErr	0.0471	0.0145	0.0137	0.0133	0.0134	**0.0125**
	AB(9,9)/$\sigma = 10$	PSNR	31.58	39.35	39.02	40.04	39.57	**40.44**
		SSIM	0.370	0.753	0.745	0.773	0.774	**0.783**
		ReErr	0.0474	0.0194	0.0201	0.0179	0.0189	**0.0171**
Man	AB(5,5)/$\sigma = 1$	PSNR	42.02	51.10	50.87	50.79	50.61	**51.27**
		SSIM	0.747	0.889	0.899	0.887	0.896	**0.899**
		ReErr	0.0177	0.0062	0.0064	0.0065	0.0066	**0.0061**
	AB(9,9)/$\sigma = 5$	PSNR	38.68	43.85	43.70	43.42	43.81	**44.05**
		SSIM	0.508	0.710	0.717	0.699	0.715	**0.718**
		ReErr	0.0260	0.0143	0.0146	0.0151	0.0144	**0.0140**
	AB(9,9)/$\sigma = 10$	PSNR	38.54	42.69	42.62	42.45	42.05	**42.89**
		SSIM	0.359	0.665	0.676	0.655	0.668	**0.678**
		ReErr	0.0265	0.0164	0.0165	0.0169	0.0177	**0.0160**
Plate	AB(5,5)/$\sigma = 1$	PSNR	28.41	48.20	48.50	48.41	41.25	**48.72**
		SSIM	0.793	0.942	0.951	0.958	0.923	**0.958**
		ReErr	0.0871	0.0089	0.0086	0.0087	0.0199	**0.0083**
	AB(9,9)/$\sigma = 5$	PSNR	24.61	35.66	38.57	37.61	36.19	**39.08**
		SSIM	0.531	0.902	0.906	0.903	0.811	**0.909**
		ReErr	0.1350	0.0378	0.0270	0.0302	0.0356	**0.0255**
	AB(9,9)/$\sigma = 10$	PSNR	24.60	34.54	34.05	34.86	32.72	**35.06**
		SSIM	0.386	0.861	0.867	0.867	0.783	**0.869**
		ReErr	0.1351	0.0430	0.0455	0.0415	0.0530	**0.0406**

Table 2: PSNR (dB), SSIM, ReErr for Gaussian blur.

Image	Degraded		Input	TV	Framelet	ani-iso TV	BM3D	Ours
Boat	GB(5,2)/$\sigma = 1$	PSNR	34.54	46.06	46.91	46.01	46.92	**47.25**
		SSIM	0.802	0.916	0.931	0.916	0.931	**0.931**
		ReErr	0.0408	0.0108	0.0098	0.0109	0.0098	**0.0095**
	GB(9,4)/$\sigma = 5$	PSNR	30.89	37.70	37.74	37.46	37.74	**38.31**
		SSIM	0.540	0.743	0.766	0.746	0.763	**0.774**
		ReErr	0.0621	0.0283	0.0282	0.0291	0.0282	**0.0266**
	GB(9,4)/$\sigma = 10$	PSNR	30.82	36.50	35.90	36.55	36.04	**36.91**
		SSIM	0.400	0.694	0.712	0.701	0.716	**0.721**
		ReErr	0.0626	0.0325	0.0349	0.0324	0.0343	**0.0312**
Cameraman	GB(5,2)/$\sigma = 1$	PSNR	35.98	44.40	44.25	44.26	43.98	**44.57**
		SSIM	0.768	0.887	0.899	0.894	0.897	**0.902**
		ReErr	0.0324	0.0123	0.0125	0.0125	0.0129	**0.0121**
	GB(9,4)/$\sigma = 5$	PSNR	31.98	35.83	36.57	36.32	37.84	**37.90**
		SSIM	0.516	0.735	0.744	0.745	0.746	**0.749**
		ReErr	0.0513	0.0329	0.0302	0.0311	0.0261	**0.0261**
	GB(9,4)/$\sigma = 10$	PSNR	31.92	34.06	34.33	33.92	34.44	**34.98**
		SSIM	0.341	0.693	0.693	0.707	0.706	**0.715**
		ReErr	0.0517	0.0404	0.0391	0.0408	0.0386	**0.0364**
Goldhill	GB(5,2)/$\sigma = 1$	PSNR	34.54	45.36	45.60	45.20	45.99	**46.05**
		SSIM	0.660	0.827	0.839	0.823	0.832	**0.843**
		ReErr	0.0403	0.0116	0.0113	0.0118	0.0108	**0.0107**
	GB(9,4)/$\sigma = 5$	PSNR	31.48	37.65	37.68	37.50	37.98	**38.23**
		SSIM	0.441	0.596	0.603	0.582	0.605	**0.615**
		ReErr	0.0573	0.0282	0.0281	0.0287	0.0271	**0.0262**
	GB(9,4)/$\sigma = 10$	PSNR	31.41	36.35	35.96	36.60	36.67	**37.12**
		SSIM	0.342	0.547	0.560	0.535	0.561	**0.566**
		ReErr	0.0578	0.0327	0.0342	0.0318	0.0315	**0.0300**
House	GB(5,2)/$\sigma = 1$	PSNR	37.62	49.05	48.88	49.15	49.99	**50.09**
		SSIM	0.824	0.888	0.899	0.894	0.899	**0.901**
		ReErr	0.0237	0.0063	0.0058	0.0063	0.0057	**0.0056**
	GB(9,4)/$\sigma = 5$	PSNR	32.57	41.46	40.80	41.87	41.16	**41.88**
		SSIM	0.582	0.792	0.813	0.807	0.799	**0.815**
		ReErr	0.0423	0.0152	0.0164	0.0145	0.0157	**0.0145**
	GB(9,4)/$\sigma = 10$	PSNR	32.49	38.96	38.44	38.99	38.23	**39.31**
		SSIM	0.390	0.754	0.766	0.778	0.778	**0.787**
		ReErr	0.0427	0.0203	0.0215	0.0202	0.0221	**0.0196**
Man	GB(5,2)/$\sigma = 1$	PSNR	42.95	50.93	50.60	50.53	50.01	**51.20**
		SSIM	0.786	0.890	0.898	0.883	0.893	**0.898**
		ReErr	0.0159	0.0063	0.0066	0.0066	0.0071	**0.0062**
	GB(9,4)/$\sigma = 5$	PSNR	39.40	44.26	44.07	44.07	44.07	**44.80**
		SSIM	0.538	0.711	0.717	0.699	0.718	**0.722**
		ReErr	0.0239	0.0137	0.0140	0.0140	0.0140	**0.0129**
	GB(9,4)/$\sigma = 10$	PSNR	39.22	42.70	42.69	42.94	42.07	**43.23**
		SSIM	0.382	0.673	0.683	0.663	0.678	**0.687**
		ReErr	0.0244	0.0164	0.0164	0.0159	0.0176	**0.0155**
Plate	GB(5,2)/$\sigma = 1$	PSNR	29.46	45.75	47.49	46.54	44.52	**47.77**
		SSIM	0.797	0.950	0.958	0.963	0.939	**0.963**
		ReErr	0.1026	0.0118	0.0097	0.0108	0.0136	**0.0094**
	GB(9,4)/$\sigma = 5$	PSNR	25.43	35.77	36.98	36.81	34.71	**37.31**
		SSIM	0.565	0.894	0.894	0.893	0.812	**0.894**
		ReErr	0.1229	0.0374	0.0325	0.0331	0.0422	**0.0313**
	GB(9,4)/$\sigma = 10$	PSNR	25.41	33.47	32.56	32.85	31.83	**33.57**
		SSIM	0.415	0.857	0.823	**0.864**	0.787	0.849
		ReErr	0.1231	0.0487	0.0541	0.0523	0.0588	**0.0481**

Table 3: PSNR (dB), SSIM, ReErr for motion blur.

Image	Degraded		Input	TV	Framelet	ani-iso TV	BM3D	Ours
Boat	MB(9,30)/$\sigma = 1$	PSNR	33.93	45.05	46.34	45.23	45.38	**46.48**
		SSIM	0.744	0.905	0.914	0.910	0.917	**0.917**
		ReErr	0.0437	0.0122	0.0105	0.0119	0.0117	**0.0103**
	MB(20,60)/$\sigma = 5$	PSNR	25.72	37.06	36.84	36.60	37.15	**37.19**
		SSIM	0.450	0.732	0.747	0.738	0.747	**0.750**
		ReErr	0.1126	0.0305	0.0313	0.0333	0.0302	**0.0304**
	MB(20,120)/$\sigma = 10$	PSNR	25.70	33.85	34.89	34.33	34.23	**35.15**
		SSIM	0.330	0.660	0.659	0.676	0.678	**0.678**
		ReErr	0.1128	0.0441	0.0391	0.0411	0.0423	**0.0389**
Cameraman	MB(9,30)/$\sigma = 1$	PSNR	32.27	43.44	44.32	43.39	43.72	**44.45**
		SSIM	0.713	0.889	0.896	0.899	0.895	**0.902**
		ReErr	0.0496	0.0137	0.0124	0.0138	0.0133	**0.0123**
	MB(20,60)/$\sigma = 5$	PSNR	30.51	36.83	36.61	37.10	37.07	**37.33**
		SSIM	0.481	0.734	0.755	0.754	0.742	**0.757**
		ReErr	0.0607	0.0293	0.0301	0.0284	0.0285	**0.0277**
	MB(20,120)/$\sigma = 10$	PSNR	30.26	34.27	35.72	35.70	35.16	**35.77**
		SSIM	0.313	0.686	0.668	0.685	0.680	**0.693**
		ReErr	0.0625	0.0394	0.0333	0.0339	0.0356	**0.0332**
Goldhill	MB(9,30)/$\sigma = 1$	PSNR	34.14	42.68	42.94	42.80	42.87	**43.43**
		SSIM	0.616	0.861	0.869	0.859	0.848	**0.871**
		ReErr	0.0422	0.0158	0.0153	0.0156	0.0154	**0.0146**
	MB(20,60)/$\sigma = 5$	PSNR	27.88	36.29	35.65	36.42	35.43	**36.53**
		SSIM	0.374	0.540	0.594	0.566	0.582	**0.604**
		ReErr	0.0867	0.0329	0.0354	0.0324	0.0364	**0.0323**
	MB(20,120)/$\sigma = 10$	PSNR	27.82	34.61	34.31	34.59	34.03	**34.75**
		SSIM	0.292	0.496	0.532	0.501	0.531	**0.534**
		ReErr	0.0873	0.0400	0.0414	0.0400	0.0427	**0.0398**
House	MB(9,30)/$\sigma = 1$	PSNR	32.96	49.33	49.85	49.55	49.08	**50.10**
		SSIM	0.782	0.890	0.902	0.897	0.900	**0.904**
		ReErr	0.0405	0.0061	0.0058	0.0060	0.0063	**0.0056**
	MB(20,60)/$\sigma = 5$	PSNR	30.68	38.96	38.63	39.10	38.88	**39.13**
		SSIM	0.510	0.763	0.798	0.783	0.774	**0.800**
		ReErr	0.0526	0.0203	0.0211	0.0200	0.0205	**0.0199**
	MB(20,120)/$\sigma = 10$	PSNR	30.52	36.09	37.39	37.08	36.90	**37.49**
		SSIM	0.333	0.714	0.725	**0.747**	0.732	0.736
		ReErr	0.0536	0.0282	0.0243	0.0252	0.0257	**0.0242**
Man	MB(9,30)/$\sigma = 1$	PSNR	40.89	51.44	51.76	51.17	51.66	**52.02**
		SSIM	0.719	0.889	0.892	0.886	0.886	**0.896**
		ReErr	0.0202	0.0060	0.0058	0.0062	0.0058	**0.0056**
	MB(20,60)/$\sigma = 5$	PSNR	35.49	42.66	43.45	43.27	41.33	**43.75**
		SSIM	0.504	0.717	0.707	0.715	0.709	**0.719**
		ReErr	0.0376	0.0164	0.0150	0.0153	0.0192	**0.0148**
	MB(20,120)/$\sigma = 10$	PSNR	35.20	40.16	41.11	40.37	39.71	**41.60**
		SSIM	0.342	0.648	0.649	0.643	0.650	**0.660**
		ReErr	0.0388	0.0219	0.0197	0.0214	0.0231	**0.0189**
Plate	MB(9,30)/$\sigma = 1$	PSNR	25.65	42.95	43.58	43.53	40.59	**43.96**
		SSIM	0.725	0.938	0.940	0.953	0.923	**0.954**
		ReErr	0.1198	0.0163	0.0152	0.0153	0.0215	**0.0149**
	MB(20,60)/$\sigma = 5$	PSNR	23.96	33.08	33.22	33.21	32.39	**33.53**
		SSIM	0.492	0.876	0.871	**0.880**	0.794	0.876
		ReErr	0.1454	0.0509	0.0501	0.0502	0.0551	**0.0484**
	MB(20,120)/$\sigma = 10$	PSNR	24.14	30.59	30.61	30.48	29.89	**30.89**
		SSIM	0.344	0.818	0.806	0.826	0.721	**0.831**
		ReErr	0.1480	0.0678	0.0676	0.0687	0.0735	**0.0655**

Table 4: The computation time (*sec*).

Method	Boat	Cameraman	Goldhill	House	Man	Plate
	AB(5,5)/ $\sigma = 1$	AB(7,7)/ $\sigma = 3$	GB(5,2)/ $\sigma = 1$	GB(7,3)/ $\sigma = 3$	MB(9,30)/ $\sigma = 1$	MB(15,45)/ $\sigma = 3$
TV	**0.32**	**0.43**	**0.59**	**0.59**	**4.10**	**0.89**
Framelet	8.11	14.37	8.37	13.49	20.09	11.01
ani-iso TV	4.56	4.64	4.04	4.12	8.42	5.93
BM3D	0.88	1.01	0.94	1.10	4.16	1.25
Ours	4.03	4.63	3.85	4.05	17.78	6.55

(a) Degraded: 32.45 (b) TV: 39.43 (c) Framelet: 39.39

(d) ani-iso TV: 39.06 (e) BM3D: 38.65 (f) Ours: 39.62

Figure 4: Deblurring results of AB(7,7)/$\sigma = 3$ for Cameraman with zoomed regions and PSNR values.

We present visual results of image deblurring. In particular, we consider AB(7,7)/$\sigma = 3$ for Cameraman/House, GB(7,3)/$\sigma = 3$ for Boat/Man, and MB(15,45)/$\sigma = 3$ for Plate/Goldhill. Figures 4-9 show that the proposed method yields the best image quality in terms of removing noises, preserving edges, and maintaining image sharpness. On the other hand, we observe stair-casing artifacts in TV and ani-iso TV. It seems that the framelet method can not completely remove the noise, while the BM3D method results in ringing artifacts.

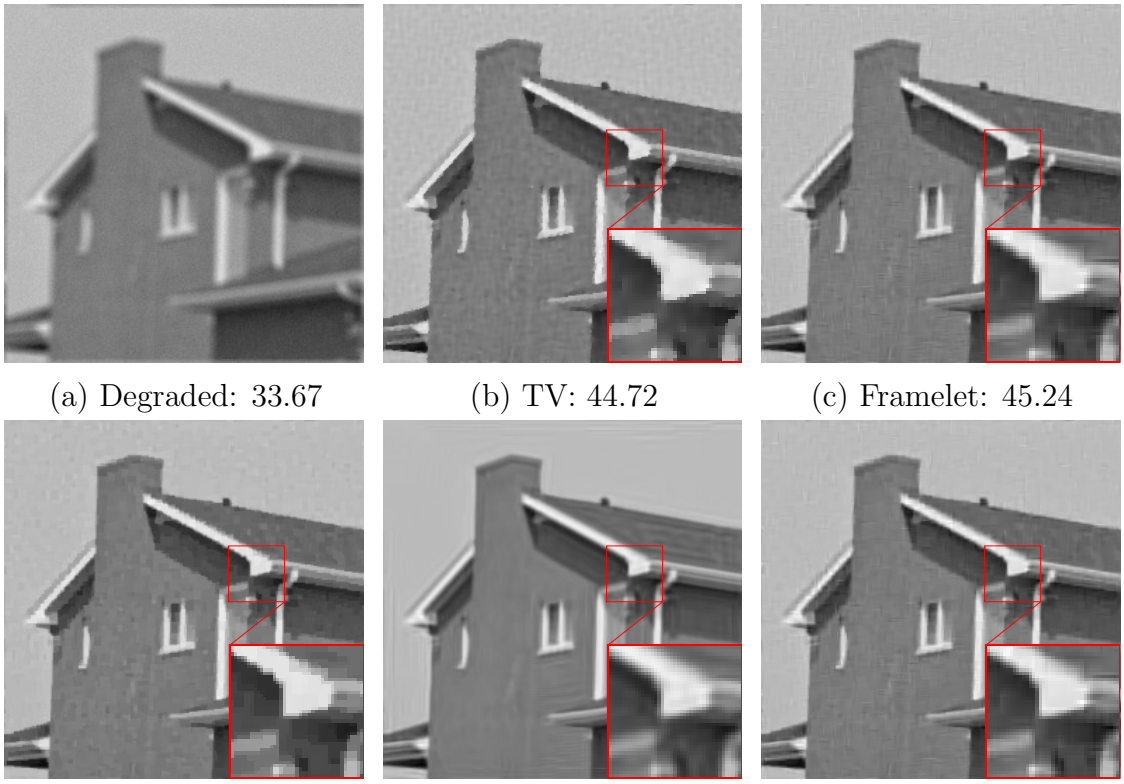

(a) Degraded: 33.67 (b) TV: 44.72 (c) Framelet: 45.24

(d) ani-iso TV: 44.43 (e) BM3D: 44.93 (f) Ours: 45.33

Figure 5: Deblurring results of AB(7,7)/σ = 3 for House with zoomed regions and PSNR values.

5. Conclusions

In this paper, we proposed a novel model in combination of an image sharpening operator and a framelet regularization for image deblurring. We proved the existence and uniqueness of the model solution under a mild condition. Furthermore, we adopted the semi-proximal ADMM (sPADMM) algorithm to find the solution and provided the convergence analysis. We conducted extensive experiments on different types of blurring kernels and different amounts of Gaussian noises, showing that the proposed approach is robust and outperforms the state-of-the-art in image deblurring. Future works include acceleration of the current workflow and possible extensions to other types of noises such as impulse noise, mixed noise, and unknown type of noise.

Acknowledgments

We are grateful to the reviewers and editors for their constructive and thoughtful comments, which greatly improved the quality of this paper. We would also acknowledge Dr. Defeng Sun from the Hong Kong Polytechnic University for helpful suggestions and discussions on the sPADMM algorithm. The research of Yifei Lou is partially supported by NSF CAREER 1846690. The research of Guoxi Ni is partially supported

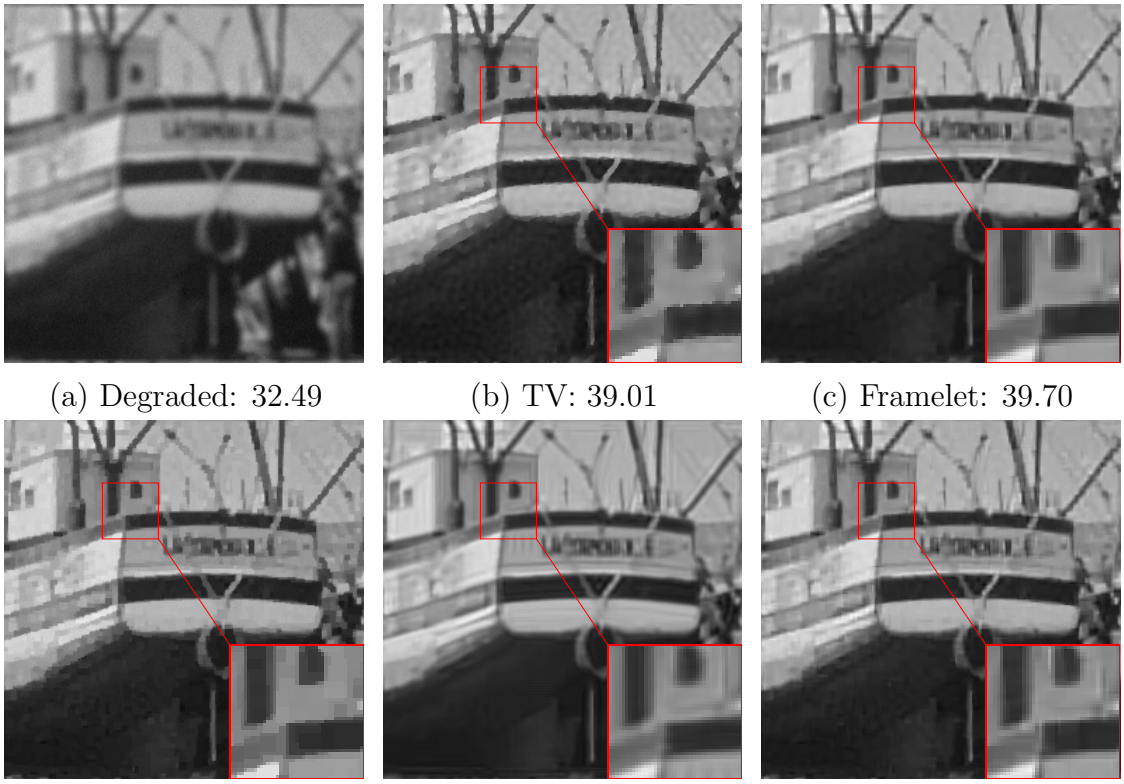

(a) Degraded: 32.49 (b) TV: 39.01 (c) Framelet: 39.70

(d) ani-iso TV: 38.92 (e) BM3D: 39.32 (f) Ours: 40.43

Figure 6: Deblurring results of GB(7,3)/σ = 3 for Boat with zoomed regions and PSNR values.

by Science Challenge project TZ2016002, NSFC(No.11171154,11671050,11771055) and 3D numerical simulation platform TB14-1 of China academy of engineering physics. The research of Tieyong Zeng is supported by National Science Foundation of China N0. 11671002, CUHK start-up and CUHK DAG 4053296, 4053342, RGC 14300219, and NSFC/RGC N_CUHK 415/19.

Appendix: Convergence proof

To make the paper self-contained, we establish the linear-rate convergence of Algorithm 1 for the minimization problem (3.2). The proof follows the work of [20].

We denote $F(u) = \frac{\lambda}{2}\|Au - f\|_2^2$, $G(d) = \|d\|_1$, $H(z) = \mu\|z\|_1$. It follows from [66] that $(\bar{u}, \bar{d}, \bar{z})$ is an optimal solution of the problem (3.3) if and only if there exists Lagrange multipliers $\bar{b}, \bar{z}$ such that

$$\begin{aligned} &-W^T\bar{b} - \bar{c} \in \partial F(\bar{u}),\ \bar{b} \in \partial G(\bar{d}),\ \bar{c} \in \partial H(\bar{c}), \\ &W\bar{u} - \bar{d} = 0,\ \bar{u} - g - \bar{z} = 0, \end{aligned} \tag{5.1}$$

where $\partial F, \partial G, \partial H$ are the subdifferential mappings of F, G, H, respectively. Therefore,

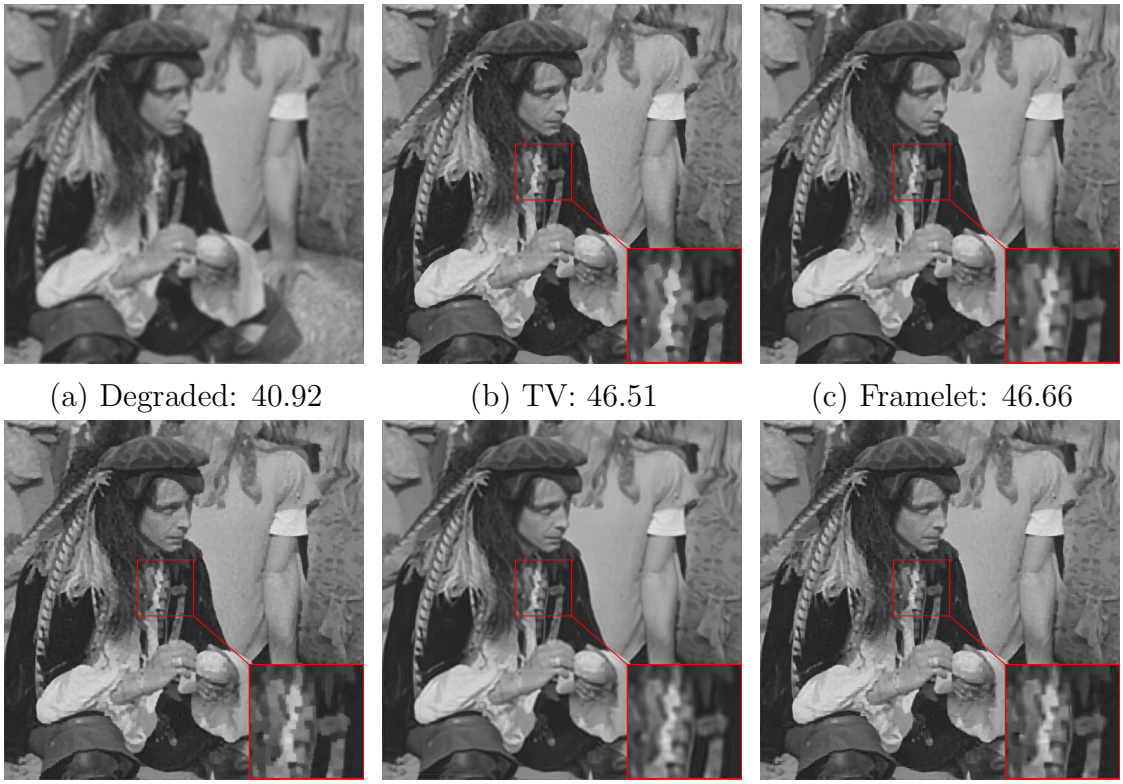

(a) Degraded: 40.92 (b) TV: 46.51 (c) Framelet: 46.66

(d) ani-iso TV: 46.62 (e) BM3D: 46.17 (f) Ours: 47.26

Figure 7: Deblurring results of GB(7,3)/$\sigma = 3$ for Man with zoomed regions and PSNR values.

we call $(\bar{u}, \bar{d}, \bar{z}, \bar{b}, \bar{c})$ the KKT point of (3.4), which satisfies the following KKT conditions:

$$\begin{cases} 0 \in \partial F(u) + W^T b + c \\ 0 \in \partial G(d) - b \\ 0 \in \partial H(z) - c \\ 0 = Wu - d \\ 0 = u - g - z. \end{cases} \tag{5.2}$$

Since the subdifferential mappings of the closed convex functions are maximal monotone [58], there exist self-adjoint and positive semidefinite operators $\Sigma_F, \Sigma_G, \Sigma_H$ such that for all $u, \hat{u} \in dom(F)$, $w \in \partial F(u)$, and $\hat{w} \in \partial F(\hat{u})$,

$$F(u) \geq F(\hat{u}) + \langle \hat{w}, u - \hat{u} \rangle + \frac{1}{2}\|u - \hat{u}\|^2_{\Sigma_F}, \langle w - \hat{w}, u - \hat{u} \rangle \geq \|u - \hat{u}\|^2_{\Sigma_F}, \tag{5.3}$$

for all $d, \hat{d} \in dom(G)$, $x \in \partial G(d)$, and $\hat{x} \in \partial G(\hat{d})$,

$$G(d) \geq G(\hat{d}) + \langle \hat{x}, d - \hat{d} \rangle + \frac{1}{2}\|d - \hat{d}\|^2_{\Sigma_G}, \langle x - \hat{x}, x - \hat{x} \rangle \geq \|x - \hat{x}\|^2_{\Sigma_G}, \tag{5.4}$$

and for all $z, \hat{z} \in dom(H)$, $y \in \partial H(z)$, and $\hat{y} \in \partial H(\hat{z})$,

$$H(z) \geq H(\hat{z}) + \langle \hat{y}, z - \hat{z} \rangle + \frac{1}{2}\|z - \hat{z}\|^2_{\Sigma_H}, \langle y - \hat{y}, z - \hat{z} \rangle \geq \|z - \hat{z}\|^2_{\Sigma_H}. \tag{5.5}$$

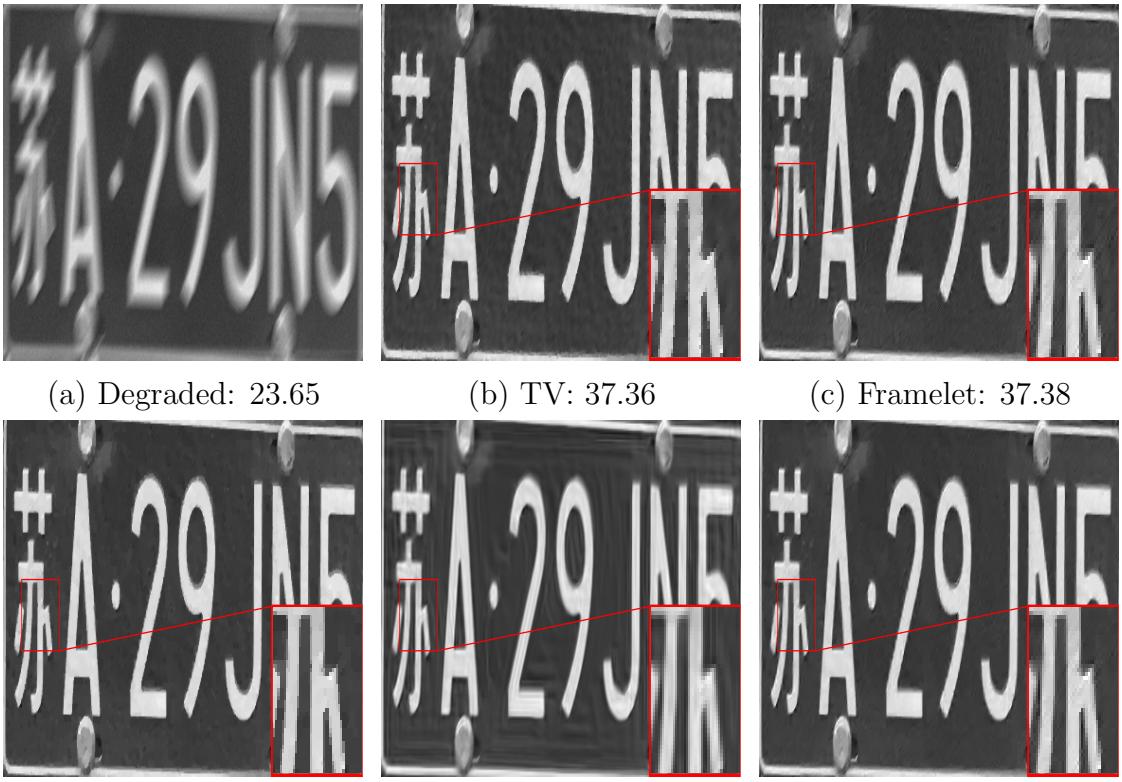

(a) Degraded: 23.65 (b) TV: 37.36 (c) Framelet: 37.38

(d) ani-iso TV: 37.75 (e) BM3D: 37.33 (f) Ours: 38.03

Figure 8: Deblurring results of MB(15,45)/$\sigma = 3$ for Plate with zoomed regions and PSNR values.

Denote $\{(u^k, d^k, z^k, b^k, c^k)\}$ be the sequence obtained from sPADMM and hence it satisfies

$$\begin{cases} 0 & \in \partial F(u^{k+1}) + W^T(\mu_1(Wu^{k+1} - d^k) + b^k) \\ & +(\mu_2(u^{k+1} - g - z^k) + c^k) + S_1(u^{k+1} - u^k) \\ 0 & \in \partial G(d^{k+1}) - (\mu_1(Wu^{k+1} - d^{k+1}) + b^k) + S_2(d^{k+1} - d^k) \\ 0 & \in \partial H(z^{k+1}) - (\mu_2(u^{k+1} - g - z^{k+1}) + c^k) + S_3(z^{k+1} - z^k) \\ 0 & = \epsilon_1(u^{k+1}, d^{k+1}) - (\eta\mu_1)^{-1}(b^{k+1} - b^k) \\ 0 & = \epsilon_2(u^{k+1}, z^{k+1}) - (\eta\mu_2)^{-1}(c^{k+1} - c^k), \end{cases} \tag{5.6}$$

where $\epsilon_1(u, d) = Wu - d$, $\epsilon_2(u, z) = u - g - z$. We further denote $u_e^k = u^k - \bar{u}$, similarly $d_e^k, z_e^k, b_e^k, c_e^k$, and

$$\begin{cases} w_1^{k+1} = b^{k+1} + (1-\eta)\mu_1\epsilon_1(u^{k+1}, d^{k+1}) + \mu_1(d^{k+1} - d^k) \\ w_2^{k+1} = c^{k+1} + (1-\eta)\mu_2\epsilon_2(u^{k+1}, z^{k+1}) + \mu_2(z^{k+1} - z^k) \\ x^{k+1} = b^{k+1} + (1-\eta)\mu_1\epsilon_1(u^{k+1}, d^{k+1}) \\ y^{k+1} = c^{k+1} + (1-\eta)\mu_2\epsilon_2(u^{k+1}, z^{k+1}). \end{cases}$$

It is straightforward to have

$$\epsilon_1(u_e^{k+1}, d_e^{k+1}) = \epsilon_1(u^{k+1}, d^{k+1}) = (\eta\mu_1)^{-1}(b^{k+1} - b^k) = (\eta\mu_1)^{-1}(b_e^{k+1} - b_e^k),$$

$$\begin{aligned} \epsilon_2(u_e^{k+1}, z_e^{k+1}) &= \epsilon_2(u^{k+1}, z^{k+1}) - g = (\eta\mu_2)^{-1}(c^{k+1} - c^k) - g \\ &= (\eta\mu_2)^{-1}(c_e^{k+1} - c_e^k) - g. \end{aligned}$$

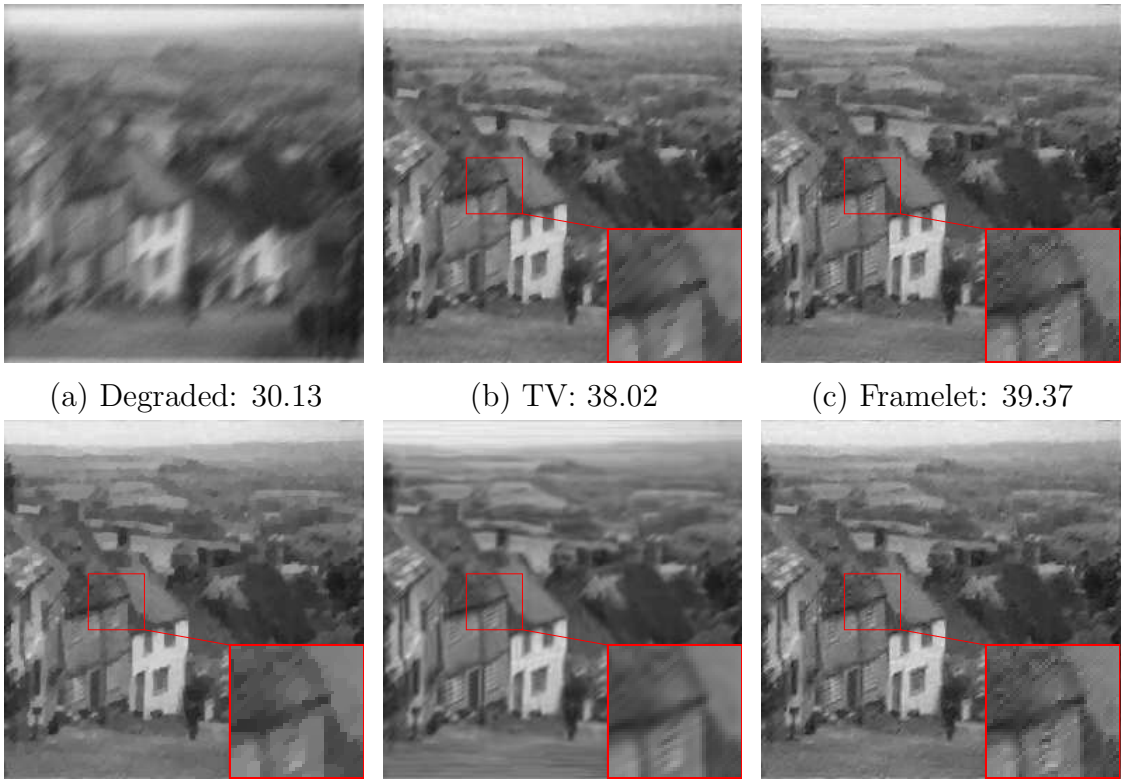

(a) Degraded: 30.13 (b) TV: 38.02 (c) Framelet: 39.37

(d) ani-iso TV: 38.22 (e) BM3D: 38.94 (f) Ours: 39.65

Figure 9: Deblurring results of MB(15,45)/$\sigma = 3$ for Goldhill with zoomed regions and PSNR values.

Combining (5.3)–(5.5) with (5.1) and (5.6), we have

$$\begin{aligned}
\|u_e^{k+1}\|_{\Sigma_F}^2 &\le \langle -W^T w_1^{k+1} - w_2^{k+1} - S_1(u^{k+1}-u^k) - (-W^T\bar{b}-\bar{c}), u_e^{k+1}\rangle,\\
\|d_e^{k+1}\|_{\Sigma_G}^2 &\le \langle x^{k+1} - S_2(d^{k+1}-d^k) - \bar{b}, d_e^{k+1}\rangle,\\
\|z_e^{k+1}\|_{\Sigma_H}^2 &\le \langle y^{k+1} - S_3(z^{k+1}-z^k) - \bar{c}, z_e^{k+1}\rangle.
\end{aligned}$$

Summing up these three inequalities and using the definitions of $w_1^{k+1}, w_2^{k+1}, x^{k+1}, y^{k+1}$, we obtain that

$$\begin{aligned}
&\|u_e^{k+1}\|_{\Sigma_F}^2 + \|d_e^{k+1}\|_{\Sigma_G}^2 + \|z_e^{k+1}\|_{\Sigma_H}^2\\
\le&(\eta\mu_1)^{-1}\langle b_e^{k+1}, b_e^k - b_e^{k+1}\rangle + (\eta\mu_2)^{-1}\langle c_e^{k+1}, c_e^k - c_e^{k+1}\rangle\\
&-(1-\eta)\mu_1\|\epsilon_1(u^{k+1},d^{k+1})\|^2 - (1-\eta)\mu_2\|\epsilon_2(u^{k+1},z^{k+1})\|^2\\
&-\mu_1\langle d^{k+1}-d^k, \epsilon_1(u^{k+1},d^{k+1})\rangle - \mu_1\langle d^{k+1}-d^k, d_e^{k+1}\rangle\\
&-\mu_2\langle z^{k+1}-z^k, \epsilon_2(u^{k+1},z^{k+1})\rangle - \mu_2\langle z^{k+1}-z^k, z_e^{k+1}\rangle\\
&-\langle S_1(u^{k+1}-u^k), u_e^{k+1}\rangle - \langle S_2(d^{k+1}-d^k), d_e^{k+1}\rangle - \langle S_3(z^{k+1}-z^k), z_e^{k+1}\rangle.
\end{aligned} \tag{5.7}$$

Next, we shall estimate the terms $\mu_1\langle d^{k+1}-d^k, \epsilon_1(u^{k+1},d^{k+1})\rangle$ and $\mu_2\langle z^{k+1}-z^k, \epsilon_2(u^{k+1},z^{k+1})\rangle$. It follows from (5.6) that

$$\begin{aligned}
&x^{k+1} - S_2(d^{k+1}-d^k) \in G(d^{k+1}), \quad x^k - S_2(d^k - d^{k-1}) \in G(d^k),\\
&y^{k+1} - S_3(z^{k+1}-z^k) \in H(z^{k+1}), \quad y^k - S_3(z^k - z^{k-1}) \in H(z^k).
\end{aligned}$$

We further consider the maximal montonic property of $\partial G(\cdot)$ and $\partial H(\cdot)$, i.e.,

$$\begin{aligned}
&\langle d^{k+1}-d^k, x^{k+1}-x^k\rangle \geq \|d^{k+1}-d^k\|_{S_2} - \langle d^{k+1}-d^k, S_2(d^k-d^{k-1})\rangle\\
&\langle z^{k+1}-z^k, y^{k+1}-y^k\rangle \geq \|z^{k+1}-z^k\|_{S_3} - \langle z^{k+1}-z^k, S_3(z^k-z^{k-1})\rangle.
\end{aligned}$$

By letting $\alpha_{k+1} = -(1-\eta)\mu_1\langle d^{k+1}-d^k, \epsilon_1(u^{k+1},d^{k+1})\rangle$ and $\beta_{k+1} = -(1-\eta)\mu_2\langle z^{k+1}-z^k, \epsilon_2(u^{k+1},z^{k+1})\rangle$, we have

$$\begin{aligned}
&-\mu_1\langle d^{k+1}-d^k, \epsilon_1(u^{k+1},d^{k+1})\rangle\\
=&-(1-\eta)\mu_1\langle d^{k+1}-d^k, \epsilon_1(u^{k+1},d^{k+1})\rangle + \langle d^{k+1}-d^k, b^k-b^{k+1}\rangle\\
=&\alpha_{k+1} + \langle d^{k+1}-d^k, x^k-x^{k+1}\rangle\\
\leq&\alpha_{k+1} - \|d^{k+1}-d^k\|^2_{S_2} + \langle d^{k+1}-d^k, S_2(d^k-d^{k-1})\rangle\\
\leq&\alpha_{k+1} - \frac{1}{2}\|d^{k+1}-d^k\|^2_{S_2} + \frac{1}{2}\|x^k-x^{k-1}\|^2_{S_2}
\end{aligned} \tag{5.8}$$

and

$$-\mu_2\langle z^{k+1}-z^k, \epsilon_2(u^{k+1},z^{k+1})\rangle \leq \beta_{k+1} - \frac{1}{2}\|z^{k+1}-z^k\|^2_{S_3} + \frac{1}{2}\|y^k-y^{k-1}\|^2_{S_3}. \tag{5.9}$$

Using $b^{k+1} = b^k + (\eta\mu_1)\epsilon_1(u^{k+1},d^{k+1})$ and $c^{k+1} = c^k + (\eta\mu_2)\epsilon_2(u^{k+1},z^{k+1})$, we obtain from (5.7)-(5.9) that

$$\begin{aligned}
&2\|u_e^{k+1}\|^2_{\Sigma_F} + 2\|d_e^{k+1}\|^2_{\Sigma_G} + 2\|z_e^{k+1}\|^2_{\Sigma_H}\\
\leq&(\eta\mu_1)^{-1}(\|b_e^k\|^2 - \|b_e^{k+1}\|^2) + (\eta\mu_2)^{-1}(\|c_e^k\|^2 - \|c_e^{k+1}\|^2)\\
&-(2-\eta)\mu_1\|\epsilon_1(u^{k+1},d^{k+1})\|^2 - (2-\eta)\mu_2\|\epsilon_2(u^{k+1},z^{k+1})\|^2\\
&+2\alpha_{k+1} - \|d^{k+1}-d^k\|^2_{S_2} + \|d^k-d^{k-1}\|^2_{S_2}\\
&-\mu_1\|d^{k+1}-d^k\|^2 - \mu_1\|d_e^{k+1}\|^2 + \mu_1\|d_e^k\|^2\\
&+2\beta_{k+1} - \|z^{k+1}-z^k\|^2_{S_3} + \|z^k-z^{k-1}\|^2_{S_3}\\
&-\mu_2\|z^{k+1}-z^k\|^2 - \mu_2\|z_e^{k+1}\|^2 + \mu_2\|z_e^k\|^2\\
&-\|u^{k+1}-u^k\|^2_{S_1} - \|u_e^{k+1}\|^2_{S_1} + \|u_e^k\|^2_{S_1}\\
&-\|d^{k+1}-d^k\|^2_{S_2} - \|d_e^{k+1}\|^2_{S_2} + \|d_e^k\|^2_{S_2}\\
&-\|z^{k+1}-z^k\|^2_{S_3} - \|z_e^{k+1}\|^2_{S_3} + \|z_e^k\|^2_{S_3}.
\end{aligned} \tag{5.10}$$

For convenience, we define

$$\left\{\begin{array}{rcl}
\delta_{k+1} &=& \min\{\eta, 1+\eta-\eta^2\}\left[\mu_1\|d^{k+1}-d^k\|^2 + \mu_2\|z^{k+1}-z^k\|^2\right]\\
&&+\|d^{k+1}-d^k\|^2_{S_2} + \|z^{k+1}-z^k\|^2_{S_3}\\
t_{k+1} &=& \delta_{k+1} + \|u^{k+1}-u^k\|^2_{S_1} + 2\|u^{k+1}-\hat{u}\|^2_{\Sigma_F}\\
&&+2\|d^{k+1}-\hat{d}\|^2_{\Sigma_G} + 2\|z^{k+1}-\hat{z}\|^2_{\Sigma_H}\\
\psi_{k+1} &=& \theta(u^{k+1},d^{k+1},z^{k+1},b^{k+1},c^{k+1}) + \|d^{k+1}-d^k\|^2_{S_2} + \|z^{k+1}-z^k\|^2_{S_3},
\end{array}\right. \tag{5.11}$$

where $\theta(u,d,z,b,c) = (\eta\mu_1)^{-1}\|b-\bar{b}\|^2 + (\eta\mu_2)^{-1}\|c-\bar{c}\|^2 + \|u-\bar{u}\|^2_{S_1} + \|d-\bar{d}\|^2_{S_2} + \|z-\bar{z}\|^2_{S_3} + \mu_1\|d-\bar{d}\|^2 + \mu_2\|z-\bar{z}\|^2$. We need to discuss two cases: $\eta\in(0,1]$ and $\eta>1$, respectively.

Case I. $\eta\in(0,1]$. By using the facts that

$$2\langle d^{k+1}-d^k, \epsilon_1(u^k,d^k)\rangle \leq \|d^{k+1}-d^k\| + \|\epsilon_1(u^k,d^k)\|^2,$$

$$2\langle z^{k+1}-z^k, \epsilon_2(u^k,z^k)\rangle \le \|z^{k+1}-z^k\| + \|\epsilon_2(u^k,z^k)\|^2,$$

and the definition of $\alpha_{k+1}, \beta_{k+1}$, we can obtain from (5.10) that

$$\begin{aligned}
&\psi_{k+1} + (1-\eta)\left[\mu_1\|\epsilon_1(u^{k+1},d^{k+1})\|^2 + \mu_2\|\epsilon_2(u^{k+1},z^{k+1})\|^2\right]\\
&-\Big[\psi_k + (1-\eta)\left[\mu_1\|\epsilon_1(u^k,d^k)\|^2 + \mu_2\|\epsilon_2(u^k,z^k)\|^2\right]\Big] + t_{k+1}\\
&+\mu_1\|\epsilon_1(u^{k+1},d^{k+1})\|^2 + \mu_2\|\epsilon_2(u^{k+1},z^{k+1})\|^2 \le 0.
\end{aligned} \tag{5.12}$$

Case II. $\eta > 1$. Similarly, we have

$$\begin{aligned}
-2\langle d^{k+1}-d^k, \epsilon_1(u^k,d^k)\rangle &\le \eta\|d^{k+1}-d^k\| + \eta^{-1}\|\epsilon_1(u^k,d^k)\|^2,\\
-2\langle z^{k+1}-z^k, \epsilon_2(u^k,z^k)\rangle &\le \eta\|z^{k+1}-z^k\| + \eta^{-1}\|\epsilon_2(u^k,z^k)\|^2.
\end{aligned}$$

Therefore, it follows from (5.10) that

$$\begin{aligned}
&\psi_{k+1} + (1-\eta^{-1})\left[\mu_1\|\epsilon_1(u^{k+1},d^{k+1})\|^2 + \mu_2\|\epsilon_2(u^{k+1},z^{k+1})\|^2\right]\\
&-\Big[\psi_k + (1-\eta^{-1})\left[\mu_1\|\epsilon_1(u^k,d^k)\|^2 + \mu_2\|\epsilon_2(u^k,z^k)\|^2\right]\Big] + t_{k+1}\\
&+\eta^{-1}(1+\eta-\eta^2)[\mu_1\|\epsilon_1(u^{k+1},d^{k+1})\|^2 + \mu_2\|\epsilon_2(u^{k+1},z^{k+1})\|^2] \le 0.
\end{aligned} \tag{5.13}$$

From (5.11)-(5.13), we see immediately that the sequence $\theta(u^{k+1},d^{k+1},z^{k+1},b^{k+1},c^{k+1}) + \|d^{k+1}-d^k\|^2_{S_2} + \|z^{k+1}-z^k\|^2_{S_3}$ is bounded and

$$\begin{aligned}
&\lim_{k\to\infty} t_{k+1} = 0\\
&\lim_{k\to\infty}\|b^{k+1}-b^k\| = \lim_{k\to\infty}(\eta\mu_1)^{-1}\|\epsilon_1(u^{k+1},d^{k+1})\| = 0\\
&\lim_{k\to\infty}\|c^{k+1}-c^k\| = \lim_{k\to\infty}(\eta\mu_2)^{-1}\|\epsilon_2(u^{k+1},z^{k+1})\| = 0.
\end{aligned} \tag{5.14}$$

By using the definition of θ and t_{k+1}, the sequences of $\{\|b^{k+1}\|\}, \{\|c^{k+1}\|\}$, $\{\|u_e^{k+1}\|^2_{\Sigma_F+S_1}\}$, $\{\|d_e^{k+1}\|^2_{\Sigma_G+S_2+\mu_1 I}\}$, and $\{\|z_e^{k+1}\|^2_{\Sigma_H+S_3+\mu_2 I}\}$ are all bounded. Since both G and H are the l_1 norm, S_2, S_3 are assumed to be semi-positive definite, and $\mu_1, \mu_2 > 0$, we have $\Sigma_G + S_2 + \mu_1 I$ and $\Sigma_H + S_3 + \mu_2 I$ are positive definite and hence the sequences of $\{\|d^{k+1}\|\}$ and $\{\|z^{k+1}\|\}$ are also bounded. Since

$$\begin{aligned}
\|Wu_e^{k+1}\| &\le \|Wu_e^{k+1} - d_e^{k+1}\| + \|d_e^{k+1}\| = \|\epsilon_1(u^{k+1},d^{k+1})\| + \|d_e^{k+1}\|\\
\|u_e^{k+1}\| &\le \|\epsilon_2(u^{k+1},z^{k+1})\| + \|z_e^{k+1}\|,
\end{aligned}$$

the sequences $\{\|Wu_e^{k+1}\|\}$ and $\{\|u_e^{k+1}\|\}$ are bounded and so is the sequence $\{\|u_e^{k+1}\|^2_{\Sigma_F+S_1+\mu_1 W^TW+\mu_2 I}\}$. Since $\Sigma_F + S_1 + \mu_1 W^TW + \mu_2 I$ is positive definite, the sequence $\{\|u_e^{k+1}\|\}$ is bounded. Therefore, the sequence $\{(u^k,d^k,z^k,b^k,c^k)\}$ is bounded, which implies the existence of a convergent subsequence to a clusters point, denoted as $\{(u^{k_i},d^{k_i},z^{k_i},b^{k_i},c^{k_i})\} \to \{(u^*,d^*,z^*,b^*,c^*)\}$.

In what follows, we show that (u^*,d^*,z^*) is an optimal solution of problem (3.3), and (b^*,c^*) is corresponding Lagrange multiplier. We note from (5.14) for the following limits:

$$\begin{aligned}
&\lim_{k\to\infty}\|d^{k+1}-d^k\| = 0, \quad \lim_{k\to\infty}\|z^{k+1}-z^k\| = 0,\\
&\lim_{k\to\infty}\|u^{k+1}-u^k\|_{S_1} = 0, \ \lim_{k\to\infty}\|d^{k+1}-d^k\|_{S_2} = 0, \ \lim_{k\to\infty}\|z^{k+1}-z^k\|_{S_3} = 0.
\end{aligned} \tag{5.15}$$

By using the inequalities

$$\|Wu^{k+1} - d^k\| \leq \|Wu^{k+1} - d^{k+1}\| + \|d^{k+1} - d^k\|$$
$$\|u^{k+1} - g - z^k\| \leq \|u^{k+1} - g - z^{k+1}\| + \|z^{k+1} - z^k\|,$$

we deduce from (5.14) and (5.15) that

$$\lim_{k\to\infty} \|Wu^{k+1} - d^k\| = 0, \quad \lim_{k\to\infty} \|u^{k+1} - g - z^k\| = 0. \tag{5.16}$$

Taking limits on both sides of (5.6) along the subsequence $\{(u^{k_i}, d^{k_i}, z^{k_i}, b^{k_i}, c^{k_i})\}$ and using (5.15), (5.16), and the closedness of $\partial F,\ \partial G$ [67], we obtain that

$$-W^T b^* - c^* \in \partial f(u^*),\ b^* \in \partial g(d^*),\ c^* \in \partial h(z^*),$$
$$Wu^* - d^* = 0,\ u^* - g - z^* = 0.$$

As a result, $(u^*, d^*, z^*, b^*, c^*)$ satisfies (5.1) and hence (u^*, d^*, z^*) is an optimal solution to problem (3.3) and (b^*, c^*) is the corresponding Lagrange multipliers.

We then show the global convergence, i.e., $\{(u^k, d^k, z^k, b^k, c^k)\} \to (u^*, d^*, z^*, b^*, c^*)$ (not just subsequence convergence). Since $(u^*, d^*, z^*, b^*, c^*)$ satisfies (5.1), we could replace $(\bar{u}, \bar{d}, \bar{z}, \bar{b}, \bar{c})$ with $(u^*, d^*, z^*, b^*, c^*)$ in the above analysis. For $\eta \in (1, (1+\sqrt{5})/2)$, (5.12) and (5.13) imply that $\{\psi_{k_i} + (1-\eta)[\mu_1\|\epsilon_1(u^{k_i}, d^{k_i}) + \mu_2\|\epsilon_2(u^{k_i}, z^{k_i})\|]\} \to 0$ and $\{\psi_{k_i} + (1-\eta^{-1})[\mu_1\|\epsilon_1(u^{k_i}, d^{k_i}) + \mu_2\|\epsilon_2(u^{k_i}, z^{k_i})\|]\} \to 0$, respectively, as $k_i \to \infty$. Consequently, the sequence $\{\|\epsilon_1(u^k, d^k)\|\},\ \{\|\epsilon_2(u^k, z^k)\|\}$ converge to 0. Furthermore, we have the following limits:

$$\begin{aligned} &\lim_{k\to\infty} \theta(u^k, d^k, z^k, b^k, c^k) + \|d^{k+1} - d^k\|_{S_2}^2 + \|z^{k+1} - z^k\|_{S_3}^2 = 0 \\ &\lim_{k\to\infty} \psi_k = 0. \end{aligned} \tag{5.17}$$

Therefore, we can see that $\lim_{k\to\infty} b^k = b^*$ and $\lim_{k\to\infty} c^k = c^*$. Moreover, we obtain from (5.14) and (5.17) that

$$\begin{aligned} &\lim_{k\to\infty} (\|d_e^k\|_{\Sigma_G}^2 + \|d_e^k\|_{S_2}^2 + \mu_1\|d_e^k\|^2) \\ &+(\|z_e^k\|_{\Sigma_H}^2 + \|z_e^k\|_{S_3}^2 + \mu_2\|z_e^k\|^2) + (\|u_e^k\|_{\Sigma_F}^2 + \|u_e^k\|_{S_1}^2) = 0. \end{aligned}$$

Hence, we have $\lim_{k\to\infty} d^k = d^*$ and $\lim_{k\to\infty} z^k = z^*$. This further implies that $\lim_{k\to\infty} \|Wu_e^{k+1}\| = 0$ and $\lim_{k\to\infty} \|u_e^{k+1}\| = 0$. Therefore, we have

$$\lim_{k\to\infty} (\|u_e^k\|_{\Sigma_f}^2 + \|u_e^k\|_{S_1}^2) + \mu_1\|Wu_e^k\|^2 + \mu_2\|u_e^k\|^2 = 0, \tag{5.18}$$

which ensures that $\lim_{k\to\infty} u^k = u^*$. As a result, we have that the whole sequence $\{(u^k, d^k, z^k, b^k, c^k)\}$ converges to $\{(u^*, d^*, z^*, b^*, c^*)\}$ if $\eta \in (0, (1+\sqrt{5})/2)$.

References

[1] Andrews H and Hunt B 1977 *Digital Image Restoration* (Englewood Cliffs, NJ: Prentice-Hall)

[2] Gonzalez R and Woods R 2008 *Digital Image Processing* 3rd ed (London: Pearson)

[3] Micheli M, Lou Y, Soatto S and Bertozzi A 2014 A Linear Systems Approach to Imaging Through Turbulence *J Math Imaging Vis.* **48** 185–201

[4] Huang J, Donatelli M and Chan R 2013 Nonstationary iterated thresholding algorithms for image deblurring *Inverse Probl Imag.* **7** 717–736

[5] Koenderink J 1984 The Structure of Images *Biol. Cybern.* **50** 363–370
[6] Buades A, Coll B and Morel J 2005 A non-local algorithm for image denoising *IEEE Conference on Computer Vision and Pattern Recognition* 60–65
[7] Chan T and Shen J 2005 *Image Processing and Analysis: Variational, PDE, Wavelet, and Stochastic Methods* (Philadelphia: SIAM)
[8] Elad M and Aharon M 2006 Image denoising via sparse and redundant representations over learned dictionaries *IEEE Trans. Image Process.* **15** 3736–3745
[9] Lou Y, Zhang X, Osher S and Bertozzi A L 2010 Image Recovery via Nonlocal Operators*J SCI Comput.* **42** 185–197
[10] Ma L, Xu L and Zeng T 2017 Low rank prior and total variation regularization for image restoration *J Sci Comput.* **70** 1336–1357
[11] Zhang X, Bai M and Ng M K 2017 Nonconvex-TV Based Image Restoration with Impulse Noise Removal *SIAM J. Imaging Sci.* **10** 1627–1667
[12] Mei J, Dong Y and Huang T 2019 Simultaneous image fusion and denoising by using fractional-order gradient information *J Comput Appl Math* **351** 212–227
[13] Dong Y, Görner T and Kunis S 2015 An algorithm for total variation regularized photoacoustic imaging *Adv. Comput. Math* **41** 423–438
[14] Micchelli C, Shen L and Xu Y 2011 Proximity algorithm for image models: denoising *Inverse Probl.* **27** 045009
[15] Rudin L, Osher S and Fatemi E 1992 Nonlinear total variation based noise removal algorithm *Phys. D* **60** 258–268
[16] Osher S and Rudin L 1990 Feature-oriented image enhancement using shock filters *SIAM J. Numer Anal.* **27** 919–940
[17] Alvarez L and Mazorra L 1994 Signal and Image Restoration Using Shock Filters and Anisotropic Diffusion *SIAM J Numer Anal* **31** 590–605
[18] Gilboa G, Sochen N and Zeevi Y Y 2002 Forward-and-backward diffusion processes for adaptive image enhancement and denoising *IEEE Trans. Image Process.* **11** 689–703
[19] Calder J, Mansouri A and Yezzi A 2010 Image sharpening via sobolev gradient flows *SIAM J. Imaging Sci.* **3** 981–1014
[20] Fazel M, Pong T K, Sun D and Tseng P 2013 Hankel Matrix Rank Minimization with Applications to System Identification and Realization *SIAM J Matrix Anal A* **34** 946–977.
[21] Li M, Sun D and Toh K C 2014 A Majorized ADMM with Indefinite Proximal Terms for Linearly Constrained Convex Composite Optimization *SIAM J. Optim.* **26** 922–950
[22] Han D, Sun D and Zhang L 2015 Linear Rate Convergence of the Alternating Direction Method of Multipliers for Convex Composite Quadratic and Semi-Definite Programming *Mathmatics of Operations Research* **60** 644–658
[23] Jia T, Shi Y, Zhu Y and Wang L 2016 An image restoration model combining mixed L1/L2 fidelity term *J. Vis. Commun. Image R.* **38** 461–473
[24] Gong Z, Shen Z and Toh K C 2014 Image restoration with mixed or unknown noises *Multiscale Model Sim.* **12** 458–487
[25] Acar R and Vogel C 1994 Analysis of bounded variation penalty methods for ill-posed problems *Inverse Probl.* **10** 1217–1229
[26] Benvenuto F, La A, Theys C, Ferrari A, Lantéri H and Bertero M 2008 The study of an iterative method for the reconstruction of images corrupted by poisson and gaussian noise *Inverse Probl.* **24** 035016
[27] Chambolle A 2004 An algorithm for total variation minimization and application *J. Math. Imaging Vision* **20** 89–97
[28] Goldstein T and Osher S 2009 The Split Bregman Algorithm for L1 Regularized Problems *SIAM J. Imaging Sci* **2** 323–343
[29] Huang Y, Ng M K and Wen Y 2008 A fast total variation minimization method for image restoration *Multiscale Model Sim.* **7** 774–795

[30] Wang Y, Yang J, Yin W and Zhang Y 2008 A new alternating minimization algorithm for total variation image reconstruction *SIAM J. Imaging Sci.* **1** 248–272
[31] Yang J, Yin W, Zhang Y and Wang Y 2009 A fast algorithm for edge-preserving variational multi-channel image restoration *SIAM J. Imaging Sci.* **2** 569–592
[32] Yang J, Zhang Y and Yin W 2009 An effcient TVL1 algorithm for deblurring multichannel images corrupted by impulsive noise *SIAM J. Sci. Comput.* **31** 2842–2865
[33] Yang J, Zhang Y and Yin W 2010 A fast alternating direction method for TVL1-L2 signal reconstruction from partial Fourier data *IEEE J. Stsp* **4** 288–297
[34] Lou Y, Zeng T, Osher S and Xin J 2015 A weighted difference of anisotropic and isotropic total variation model for image processing *SIAM J. Imaging Sci* **8** 1798–1823
[35] Lou Y and Yan M 2018 Fast L1-L2 Minimization via a Proximal Operator *J. Sci. Comput.* **74** 767–785
[36] Lou Y, Yin P, He Q and Xin J 2015 Computing Sparse Representation in a Highly Coherent Dictionary Based on8Difference of L1 and L2 *J. Sci. Comput.* **34** 178–196
[37] Lou Y, Yin P and Xin J 2016 Point Source Super-resolution Via Non-convex L1 Based Methods *J. Sci. Comput.* **68** 1082–1100
[38] Yin P, Lou Y, He Q and Xin J 2015 Minimization of L1-L2 for Compressed Sensing *SIAM J. Sci. Comput.* **37** 536–563
[39] You J, Jiao Y, Lu X and Zeng T 2019 A Nonconvex Model with Minimax Concave Penalty for Image Restoration *J. Sci. Comput.* **78** 1063–1086
[40] Zhang C 2010 Nearly unbiased variable selection under minimax concave penalty *Ann. Stat.* **38** 894–942
[41] Bao C, Dong B, Hou L, Shen Z, Zhang X and Zhang X 2016 Image restoration by minimization zero norm of wavelet frame coefficients *Inverse Probl.* **32**
[42] Cai J, Ji H, Liu C and Shen Z 2012 Framelet-based blind motion deblurring from a single image *IEEE Trans. Image Process.* **21** 562–572
[43] Cai J, Osher S and Shen Z 2009 Split Bregman method and frame based image restoration *Multiscale Model Sim.* **8** 337–369
[44] Dong B, Ji H, Shen Z and Xu Y 2012 Wavelet frame based blind image inpainting *Appl. Comput. Harmon A.* **32** 268–279
[45] Choi J, Dong B and Zhang X 2017 An edge driven wavelet frame model for image restoration *Appl Comput Harmon A.*
[46] Zhang X and Zhang X 2019 A new proximal iterative hard thresholding method with extrapolation for l0 minimization *J Sci Comput* **79** 809–826
[47] Jeong T, Woo H and Yun S 2013 Frame-based Poisson image restoration using a proximal linearized alternating direction method *Inverse Probl.* **29** 075007
[48] Daubechies I, Teschke G and Vese L 2007 Iteratively solving linear inverse problems under general convex constraints *Inverse Probl Imag.* **1** 29–46
[49] Figueiredo M and Nowak R 2003 An EM algorithm for wavelet-based image restoration *IEEE Trans. Image Process.* **12** 906–916
[50] Elad M, Starck J, Querre P and Donoho D 2005 Simultaneous cartoon and texture image inpainting using morphological component analysis (MCA) *Appl. Comput. Harmon A.* **19** 340–358
[51] Starck J, Elad M and Donoho D 2005 Image decomposition via the combination of sparse representations and a variational approach *IEEE trans. image process.* **14** 1570–1582
[52] Cai J, Chan R, Shen L and Shen Z 2009 Convergence analysis of tight framelet approach for missing data recovery *Adv. Comput Math.* **31** 87–113
[53] Cai J, Chan R and Shen Z 2010 Simultaneous cartoon and texture inpainting *Inverse Probl Imag.* **4** 379–395
[54] Sundaramoorthi G, Yezzi A, Mennucci A and Sapiro G 2007 New possibilities with Sobolev active contours *Scale Space Variational Methods, Springer-Verlag.* 506–517
[55] Evans L 1998 *Partial Differential Equations* (vol. 19 of Graduate Studies in Mathematics, American

Mathematical Society)
[56] Lou Y, Kang S, Soatto S and Bertozzi A L 2013 Video stabilization of atmospheric turbulence distortion *Inverse Probl Imag.* **3** 839–861
[57] Fu H, NG M K, Nikolova M and Barlow J L 2006 Efficient minimization methods of mixed l2-l1 and l1-l1 norms for image restoration *SIAM J. Sci. Comput.* **27** 1881–1902
[58] Rockafellar R T and Wets R J 1998 *Variational Analysis* (Springer, New York)
[59] Hiriart-Urruty J B, and Lemaréchal C 1993 *Convex analysis and minimization algorithms.* (Berlin: Springer-Verlag)
[60] Badiale M and Serra E 2011 *Semilinear elliptic equations for beginners* (London: Springer)
[61] Boyd S, Parikh N, Chu E, Peleato B and Eckstein J 2011 *Found. Trends Mach. Learning* **3** 1–122
[62] Chen C, Chan R, Ma S and Yang J 2015 Inertial proximal ADMM for linearly constrained separable convex optimization *SIAM J. Imag. Sci.* **8** 2239–2267
[63] Chan R, Tao M and Yuan X 2013 Constrained total variation deblurring models and fast algorithms based on alternating direction method of multipliers *SIAM J. Imag. Sci.* **6** 680–697
[64] Gabay D and Mercier B 1976 A dual algorithm for the solution of nonlinear variational problems via finite element approximations *Comput. Math. Appl.* **2** 17–40.
[65] Serra-Capizzano S 2003 A note on anti-reflective boundary conditions and fast deblurring models *SIAM J. Sci. Comput.* **25** 1307–1325
[66] Rockafellar R T 1970 *Convex Analysis* (Princeton University Press, Princeton, NJ)
[67] Borwein J M and Lewis A S 2006*Convex Analysis and Nonlinear Optimization*, 2nd ed (Springer, New York)
[68] Dabov K, Foi A, Katkovnik V and Egiazarian K 2007 Image restoration by sparse 3D transform domain collaborative filtering *SPIE Electronic Imaging*
[69] Dabov K, Foi A, Katkovnik V and Egiazarian K 2007 Image denoising by sparse 3D transform-domain collaborative filtering *IEEE Trans. Image Process.* **16** 2080–2095
[70] Wang Z, Bovik A C, Sheikh H R and Simoncelli E P 2004 Image quality assessment: from error visibility to structural similarity *IEEE Trans. Image Process.* **13** 600–612